POLITECNICO DI TORINO

Politecnico di Torino

Master's degree course in Mechatronic Engineering

Master's Degree Thesis

A full degree-of-freedom Model Predictive Control approach to Rendez-Vous and Docking missions of small satellites

Supervisors:

Prof. Sabrina Corpino

Prof. Carlo Novara

Eng. Fabrizio Stesina

Candidate:

Federica Mincuzzi

Academic year 2020/2021

Summary

1. Introduction 6
1.1 Contest and objective 8
1.2 Spacecraft Rendezvous & Docking maneuver 13
1.3 Rendezvous & docking for large Spacecraft 17
1.4 Rendezvous & Docking for CubeSats: State of Art 19
1.5 Problem parameters 22
1.6 Reference frame 26
2. Model derivation 31
2.1 P2P Attitude Dynamics 33
2.2 Port to Port coupled Dynamics 37
2.3 Linearization 42
3. Control design 46
3.1 Requirements and assumptions 52
3.2 Nonlinear Model Predictive control 54
3.3 Simplified and linearized system 59
3.4 Simplified and not linearized system 67
3.4.1 Increasing the Prediction Horizon 79
4. Disturbances 83
4.1 Disturbances's addition to the Simulink Model 88
4.2 Simulation 90
4.3 Parameter's perturbation 95
5. Robust Analysis – Montecarlo simulations (V-bar approach) 100
Conclusion 111
References 112
Appendix 1 114
Appendix 2 124

List of figures

Figure 1- Overall System 10
Figure 2- Plant 11
Figure 3- Definition of phase angle 14
Figure 4- Acquisition of instantaneous docking axis 15
Figure 5-Docking mechanism 16
Figure 6- NASA Docking System (NDS): active androgynous variant (top) and passive interface (bottom) 18
Figure 7 - RPOD mission 19
Figure 8 – CubeSat's elements 23
Figure 9- Reference frames 27
Figure 10- Reference systems representation: Target on the left, Chaser on the right, Earth down 28
Figure 11- Hill's equations ..... **Errore. Il segnalibro non è definito.**
Figure 12 38
Figure 13- V-bar and R-bar approach 49
Figure 14 - Acquisition of the instantaneous docking axis 50
Figure 15 - Local orbital frame 51
Figure 16 – Basic Structure of MPC 56
Figure 17 - Relative Attitude 63
Figure 18 - Relative angular velocity 63
Figure 19 - Relative position 64
Figure 20 - Relative velocity 65
Figure 21- Simulink Model (Nonlinear plant) 69
Figure 22 - Relative attitude 73
Figure 23 - Relative Angular Velocity 74
Figure 24 - Relative Position 75
Figure 25 - Relative Velocity 76
Figure 26 - Tdc (control input) 77
Figure 27 - Fdc (control input) 77
Figure 28 - Relative Angular Velocity 79
Figure 29 - Relative Attitude 80
Figure 30 - Relative Position 81
Figure 31 – Relative velocity 82
Figure 32 85
Figure 33 - Overall System including disturbances 88
Figure 34 – Ephemeris computation 89
Figure 35 - Relative Attitude (with disturbances) 90
Figure 36 - Relative Angular Velocity (with disturbances) 91
Figure 37 - Relative Position (with disturbances) 92
Figure 38 - Relative Velocity (with disturbances) 93

Figure 39 - Tdc: Control input (with disturbances) 94
Figure 40 - Fdc: control input (with disturbances) 94
Figure 41 - Relative Attitude (parameter's perturbation) 96
Figure 42 - Relative Angular Velocity (parameter's perturbation) 96
Figure 43 - Relative Position (parameter's perturbation) 97
Figure 44 - Relative Velocity (parameter's perturbation) 98
Figure 45 - Tdc: Control Input (parameter's perturbation) 98
Figure 46 - Fdc: Control Input 99
Figure 47 - Relative Attitude (Step 1 - Montecarlo simulation) 101
Figure 48 - Relative Angular Velocity (Step 1 - Montecarlo simulation) 102
Figure 49 - Relative Position (Step 1 - Montecarlo simulation) 103
Figure 50 - Relative Velocity (Step 1 - Montecarlo simulation) 104
Figure 51 - Tdc: Control Input (Step 1 - Montecarlo simulation) 104
Figure 52 - Fdc: Control Input (Step 1 - Montecarlo simulation) 105
Figure 53 - Relative Attitude (Step 2 - Montecarlo simulation) 106
Figure 54 - Relative Angular Velocity (Step 2 - Montecarlo simulation) 107
Figure 55 -- Relative Position (Step 2 - Montecarlo simulation) 108
Figure 56 - Relative Velocity (Step 2 - Montecarlo simulation) 109
Figure 57 - Tdc: control input (Step 2 - Montecarlo simulation) 109
Figure 58 - Fdc: Control input (Step 2 - Montecarlo simulation) 110

List of equations

Equation 1 - Relative Angular Velocity 34
Equation 2 – Relative angular velocity 34
Equation 3 34
Equation 4 35
Equation 5 - Kinematics 36
Equation 6 – Relative position (1) 38
Equation 7 - Relative position (2) 39
Equation 8 - Relative position (3) 39
Equation 9 - Relative velocity 40
Equation 10 - Relative acceleration 41
Equation 11 - Aerodynamic Torque 84
Equation 12 - Gravity Gradient torque 85
Equation 13 – Solar Radiation Pressure 86
Equation 14 - Magnetic Torque 87

List of tables

Table 1 – Final requirements..... 52
Table 2 – First NMPC tuning (linearized system) 62
Table 3 - Second NMPC tuning (Nonlinear system) 71

Abbreviations

GNC: Guidance Navigation & Control

MPC: Model Predictive Control

SMC: Sliding Mode Control

SROC: Space Rider Observation CubeSat

RVD: Rendez-vous & Docking

LVLH: Local Vertical Local Horizontal

LTI: Linear Time Invariant

CoM: Centre of Mass

MIMO: Multiple Inputs Multiple Outputs

SISO: Single Input Single Output

1. Introduction

Recently CubeSats are experiencing an exponential growth.

CubeSats are satellites of small size (usually under 500 Kg).

Standardized platform of CubeSat can help to reduce the costs of technical developments and scientific investigations.

Thanks to the fact that in such small object there are advanced miniaturized technologies that allow to perform proximity operations, relative navigation, Earth observations, and interplanetary transfers, they are gaining, since their inception, lots of popularity in the space field.

As explained in [1] advances in micro-electronics have enabled small spacecraft to maintain performance characteristics of modern spacecraft in small packages. Those spacecrafts are cheaper to build, test and launch.

An example is constituted by Hera Mission developed by ESA, that will be launched in 2024. It consists in a spacecraft that will carry two CubeSats: the first one will perform detailed spectral measurements of two asteroids' surfaces, the second one will measure the gravity field.

There has been, during the years, lots of challenging missions. Another example is the Lunar Gateway [2] that involves the inception of deep space objects. Inceptions from outside the station is useful for monitoring it, for investigations, to detect anomalies and preventing failures.

The inception of an operative [3] spacecraft in orbit has some peculiar characteristics. The most critical aspect is in the trajectory design and motion control of the inspector relative to the target and the communication architecture.

Due to the stringent safety constraints and the accurate maneuvers required, the retrieval to a mothercraft of a CubeSat has never been done before.

Any collision with the target must be avoid, the trajectory must be maintained out of a safety ellipse, and quick maneuvers must be used to go away from the target in case of risk of collision. Due to these reasons, there are many aspects to investigate for these kinds of missions and a high degree of accuracy is required.

Space proximity maneuvers are extremely delicate and requires high precision.

Attitude and position control are of primary importance since a spacecraft is subject to many disturbances.

The position and the velocity describe the translational motion of the center of mass of the S/C and are the subject of the orbit analysis or of the space navigation; the orbit or trajectory is the spacecraft's path in space.

The attitude and attitude rate describe the rotational motion of the body of the S/C about the center of mass and are the subject of the attitude analysis or spacecraft dynamics; the attitude is the spacecraft's orientation in space.

The attitude control must be present very often because a satellite that loses attitude control will usually tumble and then lose the payload function, power on the solar arrays, and contact with the ground, instead orbit control must be less frequent because, as long as the orbit is controlled with low-thrust systems, a short-term failure will cause no damage. Gravity takes care of short-term orbit control very well. If the orbit-control system fails, the ground or the onboard system will determine that the satellite is slowly drifting from its assigned slot and a warning can be issued with adequate time to fix the problem or implement a back-up before adverse consequences occur.

1.1 Contest and objective

The specific objective of this thesis is to define a control strategy for the last part of the Rendezvous & Docking maneuver of a CubeSat of 12U (size 20 cm x 20cm x 30 cm), with a weight of around 20 kg, that has to dock to Space Rider, a new transportation system developed by Thales-Alenia for ESA, in the framework of the SROC mission developed by CubeSat Team Polito.

This kind of proximity operation requires high level of accuracy in the control of the final approach. This is true, in particular, in the considered case in which the last meters oh trajectory that separate the chaser from the target (the indicate Space Rider) have to be controlled.

The target is called in this way because it represents the passive element, that, in this case is only collaborative and must be reached by the active element, that is the chaser.

CubeSats in general require the development and validation of the corresponding Guidance, Navigation & Control (GNC) algorithms. The main task of GNC is the execution of RVD maneuvers. It has to determine the relative position and attitude providing guidance to the controller that has to control the S/C:

- Guidance function: its task is to provide at each point the set values for the state vector in time, which will then be compared with the estimated actual values, provided by the navigation function, enabling the control function to prepare the control commands.

  Depending on the maneuvers and trajectories to be implemented, the guidance function has to:

-pre-calculate boost maneuvers in terms of execution time and duration;

-generate position and velocity profiles, $\mathbf{p}(t)$ and $\mathbf{v}(t)$, in all axes for closed loop-controlled trajectories and hold points;

-generate attitude profiles $\boldsymbol{\alpha}(t)$, e.g. for spacecraft pointing towards Earth, the Sun or a target vehicle, and angular rate profiles $\boldsymbol{\alpha}^{\cdot}(t)$ for closed loop-controlled slew maneuvers (large attitude angle rotation);

-propagate the instantaneous position of the center of mass in the vehicle body frame

-according to the propellant consumption during the mission [4].

- Navigation: is the subsystem of all sensors that determines the current position and velocity of the spacecraft.
- Control: is the closed-loop control of the trajectory in this present case, not in general. It is important because it ensures the accuracy of the position and attitude which is the main thing to take in consideration during docking maneuver. Moreover, the orbit controller uses a Nonlinear Model Predictive Control (NMPC) that is an innovative controller in applications in the space world. NMPC can be adapted to plants described by non-linear equations.
- The core of the GNC is the plant because it contains the mathematical model that simulate the motion (translational and rotational) of the spacecraft.
- The actuation system has to translate the control output of the controller in physical forces, considering the limits imposed from the real propulsion system.

Attitude and position control is carried out due to the interaction of lots of elements such as:

- the rendezvous sensor for the final approach must be able to measure axial and lateral position, and the relative attitude between docking ports of the target and of the chaser.
- the actuators provide the force needed. They usually have physical limits due to misalignments and due to the available space.
- the controller that must be properly tuned to have an optimized actuator's action.

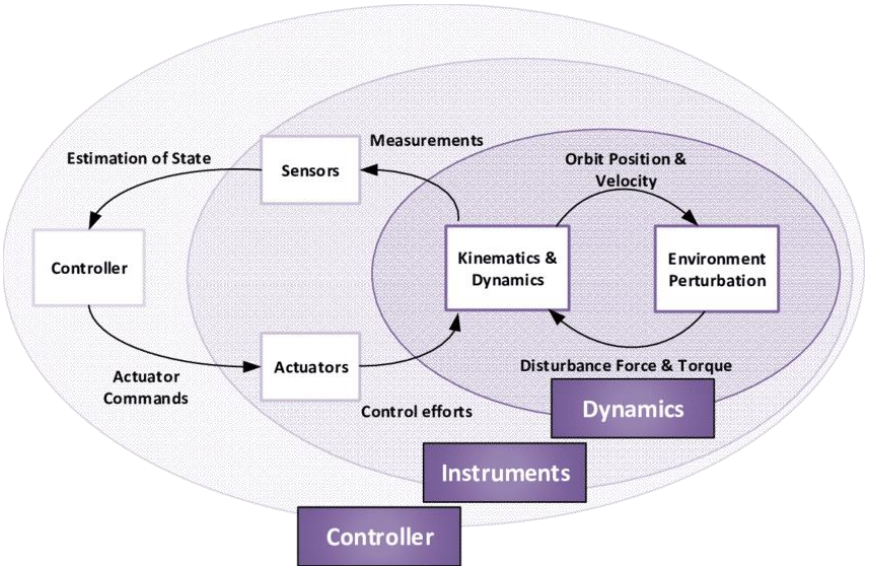

Figure 1- Overall System

Orbit control is foundamental in rendezvous or interplanetary missions, and to maintain relative position or to perform end-of-life maneuvers. In general orbit control is needed for change one or more orbital elements (i.e. to change the orbit of a satellite, the satellite's velocity vector must be changed in magnitude and/or

direction using a thruster), but for most small spacecraft orbit control is not required.

Attitude control is needed to maintain relative orientation as in rendezvous operations, to point an antenna at the ground station or other vehicle in space, to overcome perturbations and to support thermal control system and/or electrical power system. Most of spacecrafts have attitude control, because it is useful to change orientation in space (to change the attitude of a satellite, the satellite's angular rate must be changed by the application of a control torque).

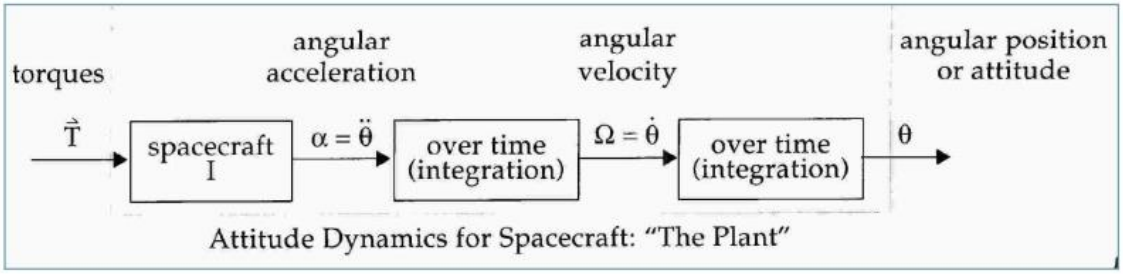

Figure 2- Plant

In the first part of the present thesis, all the disturbance that acts on the satellites are not taken in consideration.

Disturbance can be internal or environmental.

Internal disturbances are mostly due to thruster misalignments and to fuel sloshing, while noises coming from exterior are the ones related to environment properties: gravity gradient, Earth magnetic field, atmospheric drag.

The aim of the present work is to obtain the complete coupled 6 DoF port to port dynamics that will be composed by specific equations representing the relative

port to port dynamic between the docking mechanisms and the docking port, the kinematics for the relative attitude and target absolute attitude, and a modified version of the Hill's equations.

The P2P relative position dynamics describes the relative motion of the two docking ports and will be used to control the chaser during the final approach.

After a preliminary study on which is the controller to be used, and after the derivation of the above equations that describe the complete system, is possible to implement the system in Simulink, then create the controller, tune all the parameters using Matlab and simulate the overall system.

Since the complete system is really extended, the control problem is not trivial at all.

The following work of thesis has been articulated in five main chapters:

1) Introduction, contest of the mission and State of Art.
2) Derivation of the complete coupled 6 DoF port to port dynamics and linearization of the system.
3) Decision on which controller to use. Tuning of all the parameters in order to obtain the tracking of a reference trajectory.
4) Take in consideration all the disturbance forces and torques that lead to orbit variation (e.g. decay) or undesired angular acceleration and environmental and internal perturbations, such as atmospheric drag, gravity gradient and interaction with the magnetic field.
5) Montecarlo Simulations (analysis of the behavior of the system and its robustness considering different random initial condition in a certain rage).

1.2 Spacecraft Rendezvous & Docking maneuver

The rendezvous is a maneuver that is computed from two objects flying in space: typically, a spacecraft (active element) and an orbiting element around the Earth (passive element), that share the objective to approach each other.

This operation is hard because the orbital velocity and the orbit itself must coincide perfectly. The main objective of this maneuver is the docking to the other spacecraft, and this is possible due to the presence of compatible mechanism suitable for carrying out the coupling.

The chaser (passive element) in equipped with a Guidance, Navigation & Control (GNC) system that must control the states of the vehicle to allow the entry into docking phase interface.

A rendezvous mission consists of a sequence of five major phases:

- Launch and orbit injection. The chaser must be brought in the same orbital plane of the target until the achievement of stable orbital conditions. After the separation from the launcher the chaser vehicle will be on a lower orbit and maybe at an arbitrary phase angle behind the target.

- The Phasing phase has the objective of reducing the phase angle between the chaser and the target [4] because a lower orbit has a shorter orbital period. In this phase launch injection errors will be corrected. Those kinds of maneuvers are usually controlled from ground, and they are concluded once the acquisition of an initial aim point is obtained.

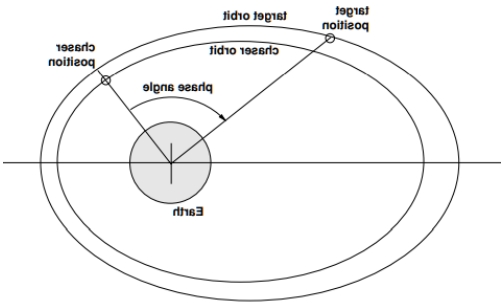

Figure 3- Definition of phase angle

- The far range rendezvous or 'homing' has the objective of the acquisition of the target orbit, the achievement of position, velocity and angular rate conditions which are necessary for the initiation of the close-range rendezvous operations, reduction of the approach velocity and the synchronization of the mission timeline with external events.
- The close-range rendezvous is divided in two subphases: the 'closing' has the objective of the reduction of the distance from the target and the achievement of conditions that allows the acquisition of the final approach corridor. At the end of this phase the chaser is ready to start the final approach, within the constraints of the safety corridor. (Considering to use the V-bar approach axis, instead of the R-bar approach axis, the closing phase may include a fly around maneuver). The second subphase is the 'final approach', where the objective is to achieve the docking conditions

in terms of position and velocity and of relative attitude and angular rates. Strong GNS system is necessary because of the fact that the actual docking axis will deviate from the nominal direction due to attitude bias, attitude control motions, and bending of the structure of the target vehicle. For this reason, is important that the chaser vehicle follows the instantaneous docking axis, and this is possible if the chaser can identify and track the center of the docking port and the direction of the docking axis. For this purpose, the rendezvous sensor for the final approach must be able to measure, in addition to axial and lateral positions, the relative attitude between the docking ports of chaser and of the target.

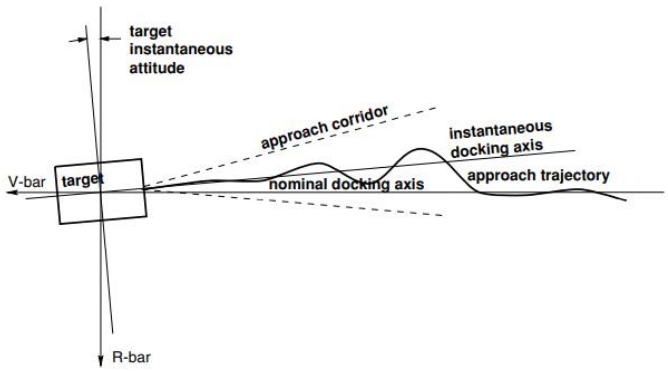

Figure 4- Acquisition of instantaneous docking axis

- The Mating phase corresponds to the docking action. This phase starts once the GNC of the chaser has managed to bring the capture interfaces of both chaser and target into reception range. There are 6 tasks that must be performed: achievement of capture, attenuation of the residual relative motion between the vehicles, bring the interfaces of the structural latches into their operational range, achieve rigid structural connection, achieve

gas-tight sealing of the connection of a pressurized passage between the vehicle and establish the connection of data, power, and fluid (propellant or water or air supply).

In docking, all tasks are concentrated in one system, the docking mechanism. The approaching vehicle is controlled to guide its capture interface into the corresponding interfaces on the target vehicle. Since at contact the two bodies will rebound and will separate again, capture must be accomplished in the short time before the interfaces have left the capture volume.

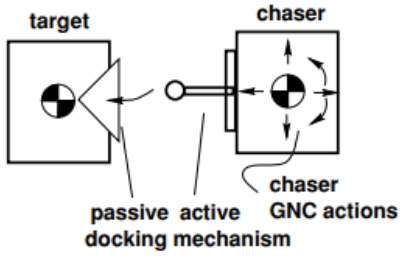

Figure 5-Docking mechanism

1.3 Rendezvous & docking for large Spacecraft

Docking is the connection between two space vehicle that connects temporary or partially permanent.

In December 1965 has been accomplish the first rendezvous maneuver when NASA launched Gemini 6A and Gemini 7. Then, in 1966 Gemini 8 and Agena Target Vehicle completed the first RVD maneuver. From that moment all those operations that required two or more collaborative vehicles become possible, so important on-orbit operations such as inspections, material and crew transfer, and others, become achievable.

In 1967 the first fully automated space docking has been performed by the Soviet Union. In this project have been used two unmanned vehicles and the docking mechanism was formed by a central probe-drogue docking system with a capturing conical interface mounted on the target and a suspended damping rod on the chaser.

In 1975 the Apollo-Soyuz Test Project had the objective to test an innovative docking mechanism. The main difference was that the docking interfaces were identical on both the spacecraft, and this was very useful to improve the system-level redundancy and the flexibility in the mission design.

In 1996 NASA developed the Advanced Docking Berthing Systems which would become the Low Impact Docking System (LIDS) in 2004.

In 2010, the LIDS became the international Low Impact Docking Systems (iLDS) or the NASA docking system

Figure 6- NASA Docking System (NDS): active androgynous variant (top) and passive interface (bottom)

In 2016 QinetiQ Space, founded by ESA tested the IBDM (International Berthing and Docking Mechanism) that is an androgynous low impact docking mechanism that is capable of docking and berthing large and small spacecraft.

1.4 Rendezvous & Docking for CubeSats: State of Art

The field of autonomous Rendezvous, Proximity Operations and Docking (RPOD) has developed rapidly in the past decade as told in [10]. The ability to dock with another spacecraft enables processes such as servicing, refueling, inspection, relocation, upgrades, and on-orbit assembly.

Conducting autonomous Rendezvous, Proximity Operations and Docking (RPOD) increases the capability of various commercial and scientific space missions.

Figure 1: RPOD Mission Phases

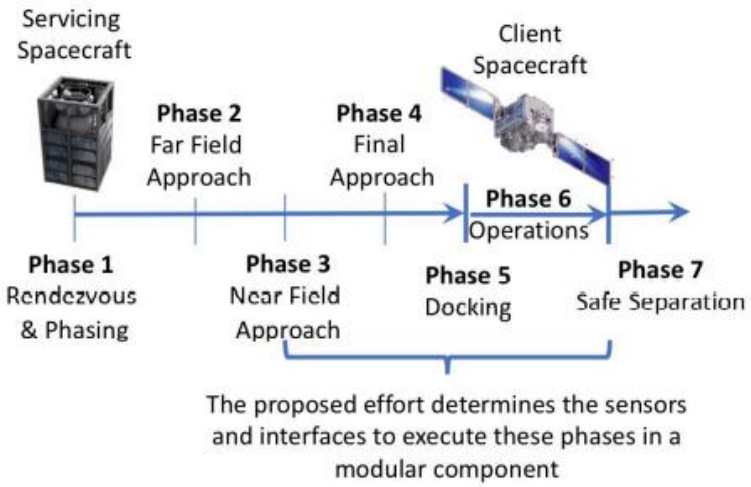

Figure 7 - RPOD mission

Referring to the concept of CubeSats, according to the ESA, the ability to autonomously rendezvous and dock CubeSats could enable in-orbit assembly of

larger structures that simply would not be possible in any other way. The biggest challenge that CubeSats must face is relate to the constraints of tight mass, propellant, and power. Furthermore, the control accuracy needed for docking would be on the order of a single centimeter.

All the docking systems are characterized by high alignment and attitude control requirements and particular procedures must be carefully supervised to guarantee a safe connection between the two spacecraft that are performing the docking maneuver.

The main drawback of CubeSats is related to the very limited available resources, but this limitation has been overcome thanks to the scaling of the results obtained with these small platforms to bigger systems, preserving the effectiveness of the outcomes.

In general, there are various technologies already tested in space using CubeSats, but only few experiments have been performed on docking systems.

One of the innovative ideas, as better explained in [4], is to exploit the self-alignment capability and the mutual attractive force generated by the magnetic interaction between two electromagnetic interfaces to make the docking maneuver easier and allowing to save fuel.

There are some works related to this topic.

In the contest of CPOD (CubeSat Proximity Operations Demonstration) mission, Tyvack Nano-Satellite [5] has developed a pair of two identical 3U CubeSats for maturing a Rendezvous & proximity operation. One solar panel array has been put on each vehicle to maintain a positive energy balance during the phase after the injection from the deployer. The mission utilizes cold gas propulsion autonomous maneuver planning, and during the final approach maneuver the

docking unit will use electro-magnetic forces to attract the two vehicles together and close the final 0.5 meters separation. Once in contact the docking mechanism attaches the two vehicles with mechanical fingers. The main advantage of such design is that the required accuracy for the docking is only 30 cm.

1.5 Problem parameters

This work of thesis is related to the Space Rider Observer Cube (SROC) mission where the main objective is to perform in-situ observations of a new transportation system developed by Thales-Alenia for ESA and called Space Rider.

This kind of mission has been developed to demonstrate the critical capabilities and technologies that are required to execute an inspection mission in a contest where the smallest mistake is of great importance. Due to this, high performance and safety constraints must be achieved.

The 12U CubeSat is deployed from the Space Rider cargo and it is equipped of a multispectral camera with which it must observe the biggest vehicle from its vicinity.

Is not possible to share all the details of the mission but is possible to give some peculiar characteristics to have a good understanding of the general contest.

In the figure behind is possible to see the main elements that characterize a CubeSat.

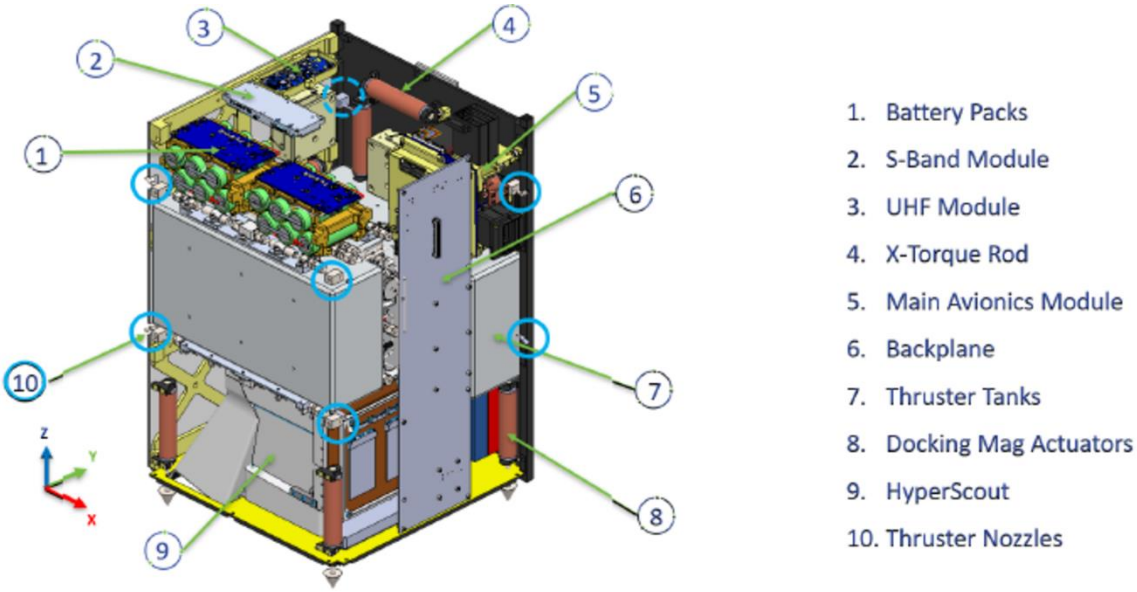

Figure 8 – CubeSat's elements

In the following tables is possible to observe the main feature of the considered mission.

Chaser properties:

Parameter	**Symbol**	**Value**
Chaser mass	mC	20 kg
Base	b	0.226 m
Height	h	0.200 m
width	w	0.366 m
Resistance coefficient	Cd	2
Basilistic coefficient	Cb	0.001

Moment of Inertia with respect to X axis	I_x	0.152 kg*m^2
Moment of Inertia with respect to Y axis	I_y	0.290 kg*m^2
Moment of Inertia with respect to Z axis	I_z	0.308 kg*m^2

Target properties:

Parameter	**Symbol**	**Value**
Target mass	mT	2000 kg
Target torque with respect to X axis	T_Ix	1500 kg/m^2
Target torque with respect to Y axis	T_Iy	1100 kg/m^2
Target torque with respect to Z axis	T_Iz	1100 kg/m^2

Orbital parameters:

Parameter	Symbol	Value
earth gravitational constant	mu	3.986 *10^14 m^3/s^2
Earth radius	Rearth	6.378137e6 m
altitude of the orbit	h	828e3 m
target position	rT	7206137 m
target orbital mean motion	w0	0.001

1.6 Reference frame

In general, the axis orientation changes according to the mission or mission phase considered. Is known that is necessary to be aware of the relative attitude of the Chaser with respect to the Target and this is studied in the body axis system.

The approach trajectories of the chaser are usually shown in the Local Orbital Frame of the target. This frame is referred as local-vertical/local-horizontal (LVLH) frame. This reference frame describes the motion of a body with respect to the center of Earth.

In the present work, X-axis is called V-bar, Y-axis is called H-bar, and Z-axis is called R-bar

The following configuration (represented in *Figure 10*) has been used:

- F_i is the Inertial Reference frame, and it is used to describe the orbital and attitude dynamics. Is centered on the Earth. The X_i axis is point towards the vernal equinox (the intersection of the Earth's equatorial plane with the plane of the Earth's orbit around the Sun). The Z_i axis is pointing towards the North pole, and the Y_i axis completes the triad. X_i and Y_i lay in the equatorial plane.
- Fo_T and Fo_c are the orbital reference frames. They are respectively the LVLH frame placed in the center of mass of the target and the LVLH frame placed in the center of mass of the chaser. They are used to represent the relative motion between two satellites or attitude pointing such as Zenith or Nadir pointing. Any satellite has its own orbital frame, typically used to represent the attitude for rendezvous type missions.
  As seen in figure, the axes are:

-Z_O: the satellite inertial position in F_i, and is referred to as R-bar;

-Y_O: the satellite inertial velocity in F_i, and is called H-bar;

-X_O: completes the direct frame and is referred to as V-bar. Considering that the chaser and the target are placed on a circular orbit, X_O goes in the direction of the velocity vector as shown in Figure 5.

The aforementioned frames are considered approximately as twins because the distance that separates them is very smaller than the length that include the radius of the Earth plus the minimum altitude of the orbit where the mission takes place. Specifically, D<<R+r.

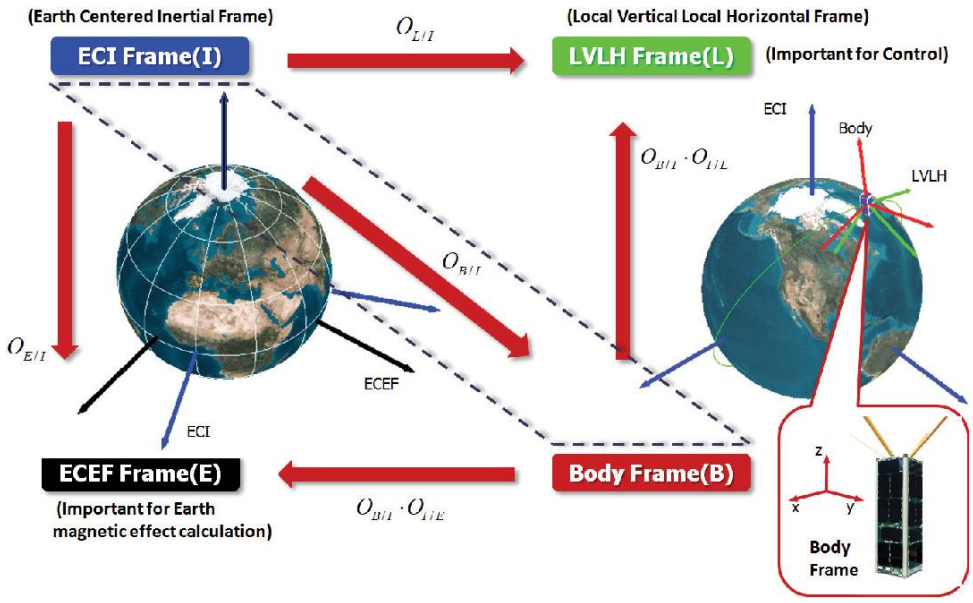

Figure 9- Reference frames

- F_{BC} and F_{BT} are the body frame respectively of the chaser and of the target. They have their origin in the satellite CoM. They are used to describe the attitude dynamics. The directions of the axis are along the

main inertia axis respectively of the chaser and of the target. $Z_{bc} = X_{bc}$ x Y_{bc} , $Z_{bt} = X_{bt}$ x Y_{bt} forming two right-handed systems. Furthermore, F_B is free to rotate in F_O.

- F_P is the target's docking port reference system in F_{BT} and F_M is the chaser docking port mechanism in F_{BC}, and they are defined in an identical way and are used to position the docking port mechanism. Their axes are positioned with respect to Fo.

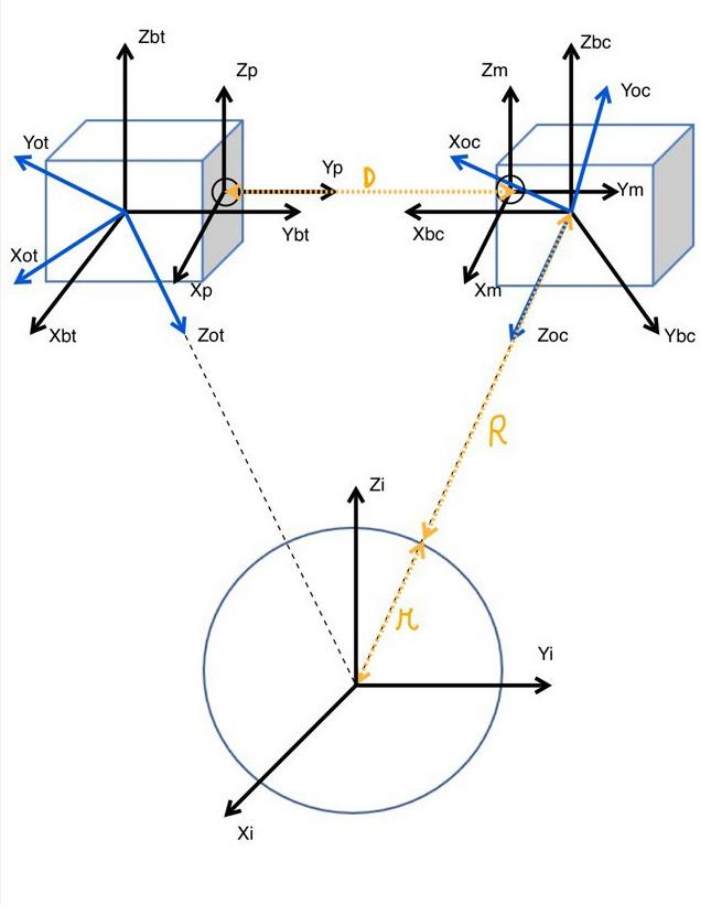

Figure 10- Reference systems representation: Target on the left, Chaser on the right, Earth down

Has been considered that between F_B and F_p there is only a translation, not a rotation for both target and chaser.

In the subsequent work will be combined the equations related to:

- the dynamics (that gives information on how F_B is rotated with respect to F_i) → $\dot{w}_{bo}^{b}$: indicates the angular velocity of the body frame with respect to the F_i expressed in F_B.

- the kinematics (that gives information on how F_B is turned with respect to F_o)→ w_{bo}^{b}: indicates the angular position of the body frame with respect F_o expressed in the body reference frame.

On this obtained equation, whose derivation will be addressed in the next chapter, the control strategy based on Nonlinear Model Predictive Control (NMPC) will be implemented.

The objective is to align the chaser with respect to the target, and to cancel the distance $\overline{OpOm}$ between the docking port and the docking mechanism. Since Clohessy-Wiltshire-Hill equations are referred to the CoM of the target and not to his docking port, those equations will not be used because R_m must be brought on R_p expressed with respect to F_{BT}.

The next chapter will address the derivation of the new system used in the sequent work.

One of the important assumptions considered here is that the distance between F_{BT} and F_p is fixed, known and has been assumed that the two centers Ot and Op are aligned so that the angle between them is 0. The same reasoning is valid for F_{BC} and F_m.

The current setup is a cooperative-target scenario. The RVD procedure is intended to take place by means of the approach along V-bar direction.

2. Model derivation

This chapter aims to the development and linearization of the non-linear 6 DoF dynamics necessary for the docking maneuver.

After the derivation of the system, will be addressed the control of the lasts 50 meters that separate the chaser from the target. The control part will be implemented using the MATLAB-Simulink® calculation software.

In this contest, will be given importance to the control of the relative attitude and position between the chaser and the target docking ports, and will be noted the strong coupling present between the dynamics of rotation and relative translation between the two bodies.

In particular, attitude (refers to the rotations) and orbit (refers to the translations) are interdependent because in low-Earth orbit, the orbit determines the spacecraft position, which determines both the atmospheric drag and the magnetic field which, in turn, affects the attitude. Traditionally this coupling has been ignored.

The complete coupled 6 DoF P2P dynamics will be composed of the following relative attitude and of a modified version of the Hill's equations.

$$\ddot{x} - 2\omega\dot{z} = \frac{1}{m_c}F_x$$
$$\ddot{y} + \omega^2 y = \frac{1}{m_c}F_y$$
$$\ddot{z} + 2\omega\dot{x} - 3\omega^2 z = \frac{1}{m_c}F_z$$

Equazione 1 - Hill's equations

The general mathematical notation w_j^{ji} represents the frame F_i in F_j expressed in F_j. Furthermore [**x**×] is the skew symmetric matrix of **x**:

$$[\boldsymbol{x}\times] = \begin{bmatrix} 0 & -x_3 & x_2 \\ x_3 & 0 & -x_1 \\ -x_2 & x_1 & 0 \end{bmatrix}$$

Instead of referring to F_p and F_m will be used the terminology respectively F_{dt} and F_{dc} referring to the docking target and the docking chaser reference frames.

2.1 P2P Attitude Dynamics

The relative attitude dynamics between the chaser's and the target's docking port is called P2P (Port to Port) attitude dynamics.

As also addressed in [8], the ports of the frame Fp (or Fdt) and Fm (of Fdc) can have any orientations in their respective body frame.

Considering the spacecraft mass, and taking into account that in this case has been considered a frame F_d in F_b with orientation A_{db} and position r_b^d, as seen in the next figure, the moment of inertia has been transformed with the 'Parallel axis theorem' in the following way:

$$I_d = A_{db}(I_b + m\,[\left|\left|r_b^d\right|\right|^2 - r_b^d r_b^{d\,T}]A_{db}^T$$

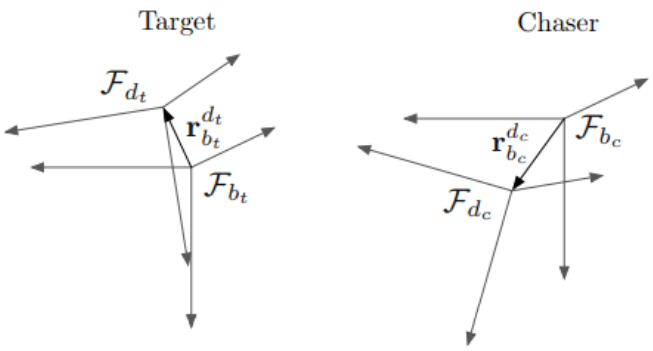

Starting from the relative attitude matrix A_{dcdt} that is mapping frame F_{dt} in F_{dc}, and from the angular velocity's composition, the relative angular velocity is:

$$w_{dc}^{dcdt} = w_{dc}^{dcO} - A_{dcdt} w_{dt}^{dtO} \qquad (1)$$

Equation 1 - Relative Angular Velocity

Where w_{dc}^{dcO} and w_{dt}^{dtO} are obtained from the absolute docking port dynamics.

Differentiating (1) with respect to time gives rise to the relative P2P dynamics that is the rotation of the chaser docking frame F_{dc} with respect to F_{dt} :

$$\dot{w}_{dc}^{dcdt} = \dot{\omega}_{dc}^{dcO} - A_{dcdt} \dot{w}_{dt}^{dtO} + [w_{dc}^{dcdt} \times](A_{dcdt}\, w_{dt}^{dtO}) \qquad (2)$$

Equation 2 – Relative angular velocity

With $\dot{w}_{dc}^{dcO}$ and $\dot{w}_{dt}^{dtO}$ given by:

$$\dot{w}_{dc}^{dcO} = Idc^{-1}[T_{dc} - (w_{dc}^{dcO} + A_{dcO}\, w_O^{OI} \times (\, Idc(w_{dc}^{dcO} + A_{dcO}\, w_O^{OI}))] \qquad (3.a)$$

$$\dot{w}_{dt}^{dtO} = Idt^{-1}[T_{dt} - (w_{dt}^{dtO} + A_{dtO}\, w_O^{OI} \times (\, Idt(w_{dt}^{dtO} + A_{dtO}\, w_O^{OI}))] \qquad (3.b)$$

Equation 3

Since a target docking port rotation influences the chaser attitude and position simultaneously, and the chaser rotation only influences the target rotation, (where one attitude variable can be expressed as a function of the other) has been removed A_{dcO} and w_{dc}^{dcO} from (3.a).

Where:

$w_O^{OI} = \begin{bmatrix} 0 \\ -wo \\ 0 \end{bmatrix}$ $where\ wo = \sqrt{\frac{\mu}{\|r_O^t\|}}$ is the target orbital mean motion.

In F_O the target position is $r_O^t = \begin{bmatrix} 0 \\ 0 \\ -r_I^t \end{bmatrix}$.

μ is the gravitational constant.

Since the chaser must actively track the target docking port, the relative dynamics must be described in F_{dc}.

Since $A_{dcO} = A_{dcdt} A_{dtO}$ and $w_{dc}^{dcO} = w_{dc}^{dcdt} + A_{dcdt} w_{dt}^{dtO}$,

(3a) becomes:

$$\dot{w}_{dc}^{dcO} = Idc^{-1}[T_{dc} - (w_{dc}^{dcdt} + A_{dcdt}\, w_{dt}^{dtO} + A_{dcdt} A_{dtO} w_O^{OI} \times (\, Idc(w_{dc}^{dcdt} + A_{dcdt}\, w_{dt}^{dtO} + A_{dcdt} A_{dtO} w_O^{OI}))] \quad (4)$$

Equation 4

And it only contains the relative P2P ad target attitude variables.

The kinematics for the relative attitude and target absolute attitude is:

$$\dot{\alpha}_{\,dcdt} = B123(\beta_{dcdt}, \gamma_{dcdt})\, w_{dc}^{dcdt} \quad (5.a)$$

$$\dot{\alpha}_{dtO} = B123(\beta_{dtO}, \gamma_{dtO})\, w_{dt}^{dcO} \qquad (5.b)$$

Equation 5 - Kinematics

Where:

$$B_{123}(\beta,\gamma) = \begin{bmatrix} \sec\beta\cos\gamma & -\sec\beta\sin\gamma & 0 \\ \sin\gamma & \cos\gamma & 0 \\ -\tan\beta\cos\gamma & \tan\beta\sin\gamma & 1 \end{bmatrix}$$

The set of non-linear equations that describe the P2P attitude is composed by (2), (3b), and (4) for the dynamics. For the kinematics, instead, the set of equations is composed by (5.a) and (5.b).

At this point the state vector is **x**= $[\alpha_{dcdt}, w_{dc}^{dcdt}, \alpha_{dtO}, w_{dt}^{dtO}]$ and the control input u= $[T_{dc}, T_{dt}]$.

- α_{dcdt} is a vector containing the three Euler angles for the relative attitude matrix A_{dcdt}.
- T_{dc}, T_{dt} respectively are the chaser's and target's control input torques.

Due to the way of building the non-linear dynamics, is evident the coupling between the target and chaser attitude.

A positive rotation of the target translates in a negative rotation for the chaser.

2.2 Port to Port coupled Dynamics

To obtain the complete 6 DoF P2P dynamics is necessary to obtain the relative position, velocity and acceleration between the chaser and the target (which represents a modified version of the Hill's equations – *Figure 11*) in addition to the previous equations (2), (3b), (5.a) and (5.b) related to kinematics and dynamics.

Unlike the classic Hill's equations, the P2P points out that a target rotation induces a chaser rotation, in order to maintain the attitude alignment, and a translation.

As seen in the following figure, the target and chaser are aligned with the orbital frame.

The docking ports are fixed with respect the body center, so r_{bc}^{dc} in F_{bc} and r_{bt}^{dt} in F_{bt} length, are fixed.

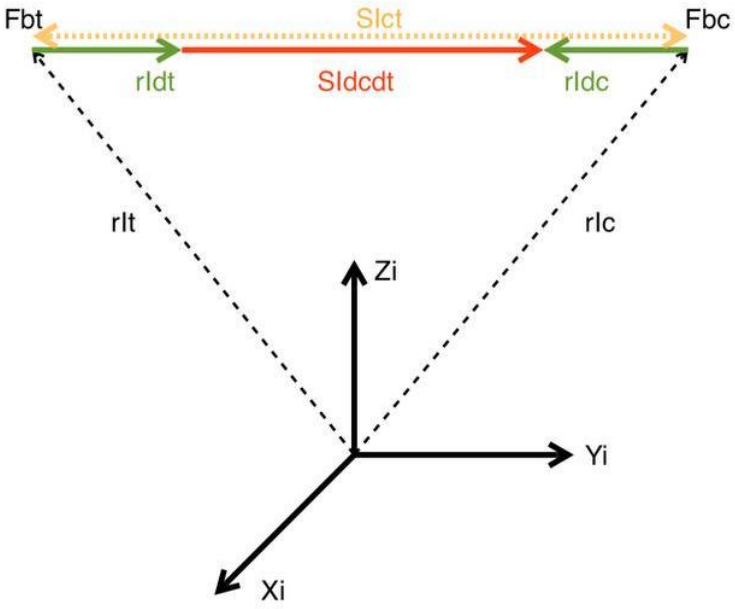

Figure 11

The P2P relative position dynamics will describe the two docking ports relative motion and will be used to control the chaser during the Final Approach.

The P2P position in the inertial frame is:

$$s_I^{dcdt}=r_I^c-r_I^t-r_I^{dt}+r_I^{dc} \quad (6)$$

Equation 6 – Relative position (1)

Where:

$r_I^c-r_I^t = s_I^{ct}$;

$r_I^{dt} = A_{Ibt}\, r_{bt}^{dt}$;

$r_I^{dc} = A_{Ibc}\, r_{bc}^{dc}$;

So (6) become:

$$s_I^{dcdt} = s_I^{ct} - A_{Ibt}\, r_{bt}^{dt} + A_{Ibc}\, r_{bc}^{dc} \quad (7)$$

Equation 7 - Relative position (2)

Where A_{Ibt} and A_{Ibc} are respectively the target's and chaser's attitude matrices in the inertial frame.

The P2P position has to be expressed in F_{dt}, therefore the P2P relative distance expressed in F_{dt} is:

$$s_{dt}^{dcdt} = A_{dtO}\, A_{OI}\, s_I^{ct} - A_{dtbt}\, r_{bt}^{dt} + A_{dtdc}\, A_{dcbc}\, r_{bc}^{dc} \quad (8)$$

Equation 8 - Relative position (3)

Where :

$A_{dtbt}\, r_{bt}^{dt} = r_{dt}^{dt}$ and $A_{dcbc}\, r_{bc}^{dc} = r_{dc}^{dc}$

Furthermore A_{dtdc} is given by the relative attitude kinematics (5.a) and A_{dtO} by the target attitude kinematics (5.b). The matrix A_{OI} is a parameter of the problem because it is determined by the target inertial position.

In order to obtain the velocity, we differentiate:

$$\dot{s}\,{}^{dcdt}_{dt} = -[w^{dtO}_{dt}\times]A_{dtO}A_{OI}s^{ct}_{I} - A_{dtO}[w^{OI}_{O}\times]A_{OI}s^{ct}_{I} + A_{dtO}A_{OI}\dot{s}^{ct}_{I} - [w^{dtdc}_{dt}\times]A_{dtdc}r^{dc}_{dc} \quad (9)$$

Equation 9 - Relative velocity

In the previous formula there has been some cancellations:

- the term $w^{dcbc}_{dc} = 0$ since there are no rotations between F_b and F_d, that means that the phase displacement is constant or null.
- As seen in *Figure 12* the distance between the center of the body frame in F_b and the docking port or the docking mechanism F_d is constant, so the term $\dot{r}\,{}^{dc}_{bc}$=0.
- Since there is no acceleration between F_O and F_I (that is fixed), the term w^{OI}_{O} is constant, so the term $\dot{w}^{OI}_{O}$=0.

In order to obtain the acceleration, another differentiation is needed and, applying some replacements, the final result is:

$$\ddot{s}\,{}^{dcdt}_{dt} = -[\dot{w}\,{}^{dtO}_{dt}\times]s^{ct}_{dt} - [w^{dtO}_{dt}\times][w^{dtO}_{dt}\times]s^{ct}_{dt} - 2[w^{dtO}_{dt}\times]\dot{s}\,{}^{dcdt}_{dt} - [A_{dtO}w^{OI}_{O}\times][A_{dtO}w^{OI}_{O}\times]s^{ct}_{dt} - 2[A_{dtO}w^{OI}_{O}\times]\dot{s}\,{}^{dcdt}_{dt} - 2[A_{dtO}w^{OI}_{O}\times][w^{dtO}_{dt}\times]s^{ct}_{dt} + 2[A_{dtO}w^{OI}_{O} + w^{dtO}_{dt}\times][AT_{dcdt}w^{dcdt}_{dc}\times]AT_{dcdt}r^{dc}_{dc} + [AT_{dcdt}\dot{w}\,{}^{dcdt}_{dc}\times]AT_{dcdt}r^{dc}_{dc} +$$

$$2[AT_{dcdt}w_{dc}^{dcdt}\times][AT_{dcdt}w_{dc}^{dcdt}\times]AT_{dcdt}r_{dc}^{dc}+\mu\frac{A_{dtO}r_O^t}{||r_0^t||}-$$

$$\mu\frac{A_{dtO}r_O^t+s_{dt}^{dcdt}-AT_{dcdt}r_{dc}^{dc}+r_{dt}^{dt}}{||A_{dtO}r_0^t+s_{dt}^{dcdt}-AT_{dcdt}r_{dc}^{dc}+r_{dt}^{dt}||_3}+AT_{dcdt}\frac{F_{dc}}{mc} \qquad (9)$$

Equation 10 - Relative acceleration

Where:

- F_{dc} is the chaser's control force that appears explicitly in the non-linear dynamics.
- $r_O^t = [0\ 0\ -r_O^t]^T$

In the previous formula (9) is represented the equations of motion in a non-inertial frame and can be identified the Coriolis and centripetal inertial accelerations due to the docking frame F_{dt} and orbital frame F_o rotations.

The state-space as the plant output y will be equal to the state x.

2.3 Linearization

The output equation of the linearized plant will be of the form

$y = Cx + Du.$

Where C is the identity matrix and D is null.

The state vector and the control input that actuate the spacecraft can be respectively defined as:

$\mathbf{x}=[\alpha_{dcdt}, w_{dc}^{dcdt}, \alpha_{dtO}, w_{dt}^{dtO}, s_{dt}^{dcdt}, \dot{s}_{dt}^{dcdt}]^T$ (10)

$u=[T_{dc}, T_{dt,} F_{dc}]^T$ (11)

where:

α_{dcdt} is the relative attitude between the docking port and the docking mechanism;

w_{dc}^{dcdt} is the relative angular velocity between the docking port and the docking mechanism;

α_{dtO} is the target relative attitude between F_{dt} and the orbital frame;

w_{dt}^{dtO} is the target relative angular velocity between F_{dt} and the orbital frame;

s_{dt}^{dcdt} is the relative P2P position between F_{dt} and F_{dt}

$\dot{s}_{dt}^{dcdt}$ is the relative P2P velocity between F_{dt} and F_{dt}

The next step will be the linearization, but before going into it, has been noted that results better using a reduced state-space dynamics that is obtained by removing the target relative attitude.

This reduced state-space dynamics can be used for any relative position/rotation.

Consequently, the new state vector and the new control input are respectively defined as:

$\mathbf{x}=[\alpha_{dcdt}, w_{dc}^{dcdt}, s_{dt}^{dcdt}, \dot{s}\,_{dt}^{dcdt}]^T$ (12)

$u=[T_{dc}, F_{dc}]^T$ (13)

In this way the model will be easier, and the simulation time will be shorter, but there will be some information related to the direct influence of the target state on the relative state that will be partially lost.

The previous state vector (12) and the control input (13), together with (2), (3b), (5a), (5b) have been linearized for simplicity. The linearization does not cause deterioration of the performance of control for the maneuvers that are considered. Thanks to linearization has been possible analyzing the system performing a stability analysis and controlling the system performing a stabilization around an equilibrium point.

$$\delta\dot{x}(t) = A\delta x(t) + B\delta u(t)$$

$$\delta y(t) = C\delta x(t) + D\delta u(t)$$

Where A, B, C, D are Jacobian matrices.

In the considered work of thesis, the A matrix will be of dimension 12x12 such as C matrix, B matrix will be of dimension 12x6 due to (12) and (13), and D matrix will be null.

After the linearization has been performed, the stability of the system has been analyzed computing the eigenvalues of the A matrix and analyzing its real part.

The linearized system approximates the nonlinear system that holds in a neighborhood of the constant input $\bar{u}$ and the equilibrium state $\bar{x}$.

The linearization has been performed around the following equilibrium points:

$\alpha_{dcdt} = w_{dc}^{dcdt} = 0$

$s_{dt}^{dcdt} = \dot{s}_{dt}^{dcdt} = 0$

$T_{dc} = F_{dc} = 0$

The used initial conditions have been the following:

• $\alpha_{dcdt} = 0$

• $r_{dc}^{dc} = [0.15\ 0\ 0]^T$ m

• $r_{dt}^{dt} = [-0.15\ 0\ 0]^T$ m

• $s_{dt}^{dcdt} = [-50\ 0\ 0]^T$ m

The state-space model for the 6 DoF port to port dynamics is

$$\dot{x} = Ax + Bu$$

$$y = Cx + Du$$

The linearization code has been reported in the Appendix 1.

Subject to the following hypothesis:

$w_{dc}^{dcdt} = \begin{bmatrix} 0 \\ 0 \\ 0 \end{bmatrix}$ Since chaser and target are not rotating.

$w_{dt}^{dtO} = \begin{bmatrix} 0 \\ 0 \\ 0 \end{bmatrix}$ because the target is only collaborative.

After the linearization, the obtained A and B matrices are the following:

A =

$$\begin{bmatrix}
0 & 0 & 0 & A14 & 0 & 0 & 0 & 0 & 0 & 0 & 0 & 0 \\
0 & 0 & 0 & 0 & A25 & 0 & 0 & 0 & 0 & 0 & 0 & 0 \\
0 & 0 & 0 & 0 & 0 & A36 & 0 & 0 & 0 & 0 & 0 & 0 \\
0 & 0 & 0 & 0 & 0 & 0 & 0 & 0 & 0 & 0 & 0 & 0 \\
0 & 0 & 0 & 0 & 0 & 0 & 0 & 0 & 0 & 0 & 0 & 0 \\
0 & 0 & A63 & A64 & 0 & 0 & 0 & 0 & 0 & 0 & 0 & 0 \\
0 & 0 & 0 & 0 & 0 & 0 & 0 & 0 & 0 & A710 & 0 & 0 \\
0 & 0 & 0 & 0 & 0 & 0 & 0 & 0 & 0 & 0 & A811 & 0 \\
0 & 0 & 0 & 0 & 0 & 0 & 0 & 0 & 2 & 0 & 0 & A1012 \\
0 & 0 & 0 & 0 & 0 & 0 & 0 & 0 & 0 & 10 & 0 & A1012 \\
0 & 0 & A113 & A114 & 0 & 0 & 0 & A118 & 0 & 0 & 10 & 0 \\
0 & A122 & 0 & 0 & 0 & 0 & A127 & 0 & A129 & A1210 & 0 & 10
\end{bmatrix}$$

$$B = \begin{bmatrix} 0 & 0 & 0 & 0 & 0 & 0 \\ 0 & 0 & 0 & 0 & 0 & 0 \\ 0 & 0 & 0 & 0 & 0 & 0 \\ A41 & 0 & 0 & 0 & 0 & 0 \\ 0 & A52 & 0 & 0 & 0 & 0 \\ 0 & 0 & A63 & 0 & 0 & 0 \\ 0 & 0 & 0 & 0 & 0 & 0 \\ 0 & 0 & 0 & 0 & 0 & 0 \\ 0 & 0 & 0 & 0 & 0 & 0 \\ 0 & 0 & 0 & A104 & 0 & 0 \\ 0 & 0 & A113 & 0 & A115 & 0 \\ 0 & A122 & 0 & 0 & 0 & A126 \end{bmatrix}$$

Where all the values from A11 to A1212 are constant parameters due to the linearization.

3. Control design

The task of the control function is to provide the force and torque commands which will be executed by the reaction control system of the spacecraft to correct the deviations of the actual state vector from the nominal one. While the guidance function provides the nominal or reference state, and the navigation function estimates the actual state, from the differences of the two states the control function produces actuation commands to compensate for the effects of disturbances and errors.

Motion control is always needed because natural and artificial disturbances must be counteracted, but there are many other reasons.

In this section will be reported the design of the controller and the way it has been built.

The rendezvous problem consists of controlling the active spacecraft so that it docks with a passive target in a circular orbit along the prescribed docking axis.

In general, the plant of the system can be divided in two main parts, which are translational and rotational dynamics/kinematics.

The main difference with respect to the other works on the same argument, has been that in this thesis, the translational and rotational parts have been coupled in the control project.

During the last stages of Rendezvous and during docking, the relative navigation mode starts, so the important information that must be known is the distance of the Chaser from the Target.

A Non-linear Model Predictive Controller has been used put in feedback to the overall system to guide and control the chasing CubeSat during the rendezvous with the passive target in a circular orbit. In general, feedback is used to overcome the effects of uncertainty. It is well-known that introducing feedback brings with it the possibility to destabilizing the system, but, at the same time it can be very effective for reducing model uncertainty and effects of disturbances. The smaller the sensitivity, the better the feedback is because the effect of the disturbance is kept small.

Using an NMPC for the overall system (translational and rotational part) has the drawback that the overall simulation is computationally more expensive in terms of time and power, and the ‘’trial and error’’ procedure is not trivial at all.

At the same time, the above choice has the big advantage of considering the couplings of the dynamics and this has better overall performance with respect to consider the variable separated.

There have been many works where MPC technique has been employed. To mention one of these works, in [11] the controller is designed to make a transition between MPC guidance during a spacecraft rendezvous phase and MPC guidance during a spacecraft docking phase, with each phase having distinct requirements, constraints, and sampling rates.

In work [12] an MPC controller has been used for each of the 3 phases in which the rendezvous maneuver has been partitioned based on the range of operation, unlike has be done in this work of thesis where, instead, has been considered only the final part of the maneuver (the lasts 50 meters). In this work [12] the MPC control system is designed to be used from the point of target detection to the point of target capture and to work in both circular and elliptical orbits. In this paper, the MPC controller has been used from the point of target detection until target capture. Instead, before of this moment, MPC has been used successfully only for trajectory tracking, and for individual spacecraft maneuvers.

An MPC controller is attractive because it re-plans the optimal trajectory at each sampling instant and because it has the intrinsic ability of handling constraint and to consider as control objective the achievement of a trajectory end-point rather than a complete trajectory, alongside the availability of well-researched models of relative dynamics that can be used for prediction. Moreover, constraints (e.g. thrust availability, passive safety requirements), and model parameters (e.g. target orbit) can be modified on-line.

The drawback is that using MPC for spacecraft is computationally complex. With respect to the limited computing available on board a spacecraft, the numerical optimizers are very more complex.

In this work of thesis, the RVD procedure is intended to take place using the approach along V-bar, which means approaching to the target horizontally, along the x-axis.

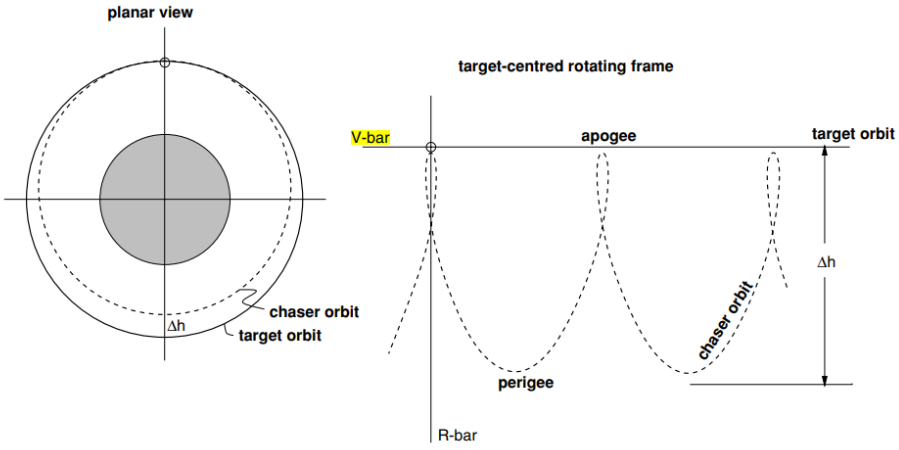

Figure 12- V-bar and R-bar approach

Is known that the close range rendezvous phase is divided into two subphases:

- a preparatory phase leading to the final approach corridor, (the 'closing')
- a final approach phase leading to the mating conditions.

For a V-bar approach there is no distinction between those two subphases because the direction of motion remains the same and no change of sensor's type occurs.

If the approach axis for mating is not in the + or − V-bar direction, instead, the closing phase may include a fly-around maneuver to acquire the approach axis.

The actual docking axis will deviate from the nominal direction due to attitude bias, attitude control motions, and bending of the structure of the target vehicle. For this reason, is important that the chaser vehicle acquires and follows the instantaneous docking axis (as seen in the *Figure 14*).

This is possible only when the chaser has the navigation means to identify and track the center of the docking port and the direction of the docking axis.

For this purpose, the rendezvous sensor for the final approach must be able to measure, in addition to axial and lateral positions, the relative attitude between the docking ports of the chaser and of the target.

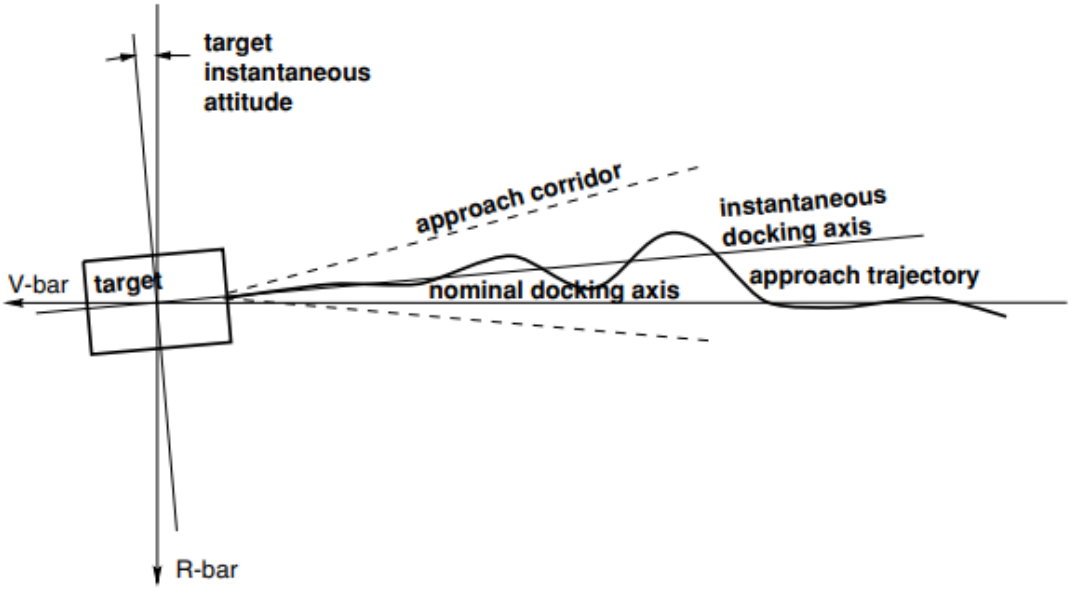

Figure 13 - Acquisition of the instantaneous docking axis

In general, as seen in the following figure the coordinate a1 = a2 × a3 (that is in the direction of the orbital velocity vector but not necessarily aligned with it) in the rendezvous literature is also called V-bar.

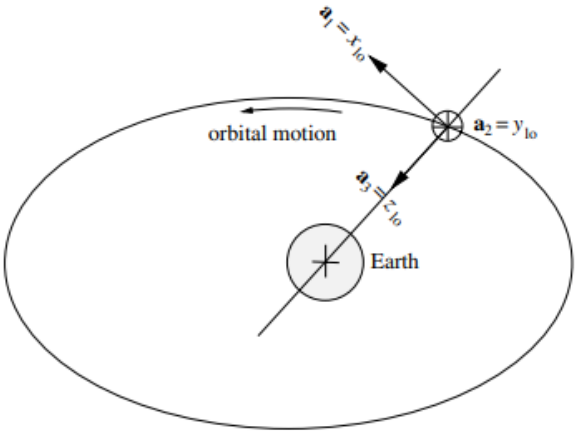

Figure 14 - Local orbital frame

3.1 Requirements and assumptions

This work of thesis has been based on some assumptions:

- A CubeSat (Chaser) of 12U is considered (20 cm x 20 cm x 30 cm), with mass mc=20 Kg, and a Target vehicle of mass mt=2000 Kg.
- In the present thesis is considered that the control starts at 50 meters of distance between the Chaser and the Target when the Chaser is already aligned to the Target. In this way has been possible to consider a strategy of guidance based on straight-line approaches without fly around maneuvers. Obviously, this phase of the mission depends on the previous ones, so this consideration implies that there can be uncertainty on the real position and velocity of the CubeSat in the Hold Point (HP) at 50 meters.
- As already said, the distance between the docking port O_m and the Chaser CoM that is O_{bc}, and the docking mechanism O_p and the Target CoM O_{bt} has been considered respectively fixed.

In general, as also seen in [14], the controller has the goal of reaching the soft docking performance under safety constraints reported in the following table:

Required Performance
Approach velocity [m/s] <0.02
Lateral alignment [m] <0.01
Lateral velocity [m/s] <0.01

Table 1 – Final requirements

The requirements to be met at the end docking, i.e. at the start of coupling, are:

- Lateral alignment of less than 0.01 m must be respected;
- Approach velocity at contact of less than 0.02 m/s must be respected at the end of docking;
- Lateral velocity (along V-bar and H-bar axes) at contact of less than 0.01 m/s must be respected at the start of coupling;
- Relative attitude at contact of less than 1 deg;
- Relative angular velocity of less than 0.1 deg at contact.

According to the strategies defined for any phase, the controller must control the relative velocity, the relative position, the relative attitude, and angular velocity.

The Non-Model Predictive Control will be utilized, and it will be useful to track the reference trajectory, to consider constraints on the fuel consumption, safety conditions of the maneuver and time to capture.

Is important to highlight that the prediction of the future states leads to the definition of the optimal trajectory.

3.2 Nonlinear Model Predictive control

As explained in [7], traditionally Rendezvous and proximity maneuvers have been performed using open-loop maneuver and ad hoc error correction. However, in the latest years Nonlinear Model Predictive Control (NMPC) is gaining interest even for Control and Rendezvous & Docking maneuvers. Thanks to the MPC approach, the various constraints arising in these maneuvers can be handled. Constraints on spacecraft positioning within Line-of-Sight cone while approaching the docking port on the target platform, and constraints on approach velocity to match the velocity of the docking port. In general, we can observe that this kind of feedback control approach can be useful to satisfy various maneuver's requirements, to provide robustness to disturbance and to reduce fuel consumption.

NMPC is a general flexible approach to control nonlinear systems, and it allows to deal with input/state/output constraints and to manage systematically the trade-off performance/command effort.

Sometimes, in order to have better performance, is necessary to have a high command activity, but this means having an higher energy consumption.

At each time step, a prediction over a given time horizon is performed using a model of the plant, and the command input is chosen as the one yielding the best prediction that gives the desired behavior.

In general, MPC is a control method that is faced according to the Receding Horizon principle: every sampling instant (Prediction Horizon) an optimized sequence of input capable of minimizing a cost function is found. Only the first control action is fed to the system, while the others are discarded. This procedure is repeated for every sampling instant until the one corresponding to the value of the Prediction Horizon is reached. This new optimization problem must be solved for every sampling interval, and this create a real time closed-loop controller.

NMPC is based on two key operations: prediction and optimization.

A model of the plant has been used to make a prediction of the system behavior over a given time interval. At each time $t=t_k$, the system state and output are predicted over the time interval [t, t+Tp], where Tp>Ts (sampling time) is the prediction horizon.

The prediction is obtained by integration of the following MIMO nonlinear system:

$$\dot{x} = f(x, u)$$

$$y = h(x, u)$$

At any time T, the predicted output $\hat{y}(T)$ is a function of the initial state x(t) and of the input signal in the interval [t, T] that is u(t:T).

At each time $t=t_k$, an input signal u*(t: T) has been looked so that the prediction has the desired behavior for $T \in [t,t+Tp]$.

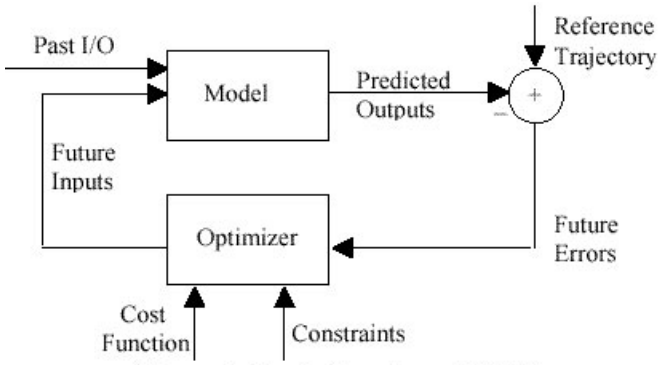

Figure 15 – Basic Structure of MPC

The concept of desired behavior is formalized by defining the following objective function or cost function that is a function of the input signal and of the predicted tracking error that is the difference between the reference signal and the predicted output:

$$J\big(u(t{:}\,t+Tp)\big) = \int_{t}^{t+Tp} (\big|\big|\widetilde{y_p}(\mathrm{T})\big|\big|_Q^2 + ||u(\mathrm{T})||_R^2)d\mathrm{T} + \big|\big|\widetilde{y_p}(t+Tp)\big|\big|_P^2$$

Where:

- $\big|\big|\widetilde{y_p}(\mathrm{T})\big|\big|_Q^2$ is the weighted norm of the vector of the tracking error. In particular $\widetilde{y_p}(\mathrm{T})$ =r(T) - $\hat{y}(\mathrm{T})$ is the predicted tracking error;
- r(T) is the reference to track;
- $||.||_x$ are weighted vector norms and their integrals are signal norms;
- $\big|\big|\widetilde{y_p}(t+Tp)\big|\big|_P^2$ is the predicted tracking error at the final time of the interval, so it gives further importance to the "final" tracking error;
- The input signal u*(t: t +Tp) is chosen as the one minimizing the objective function $J\big(u(t{:}\,t+Tp)\big)$;

- The goal is the minimization of the tracking error sequence norm $||\widetilde{y_p}(\mathrm{T})||_Q^2$, at each time t_k over a finite time interval;
- The term $||u(\mathrm{T})||_R^2$ allows to menage the trade-off between performance and command activity.

Considering to be at time t, the state has been measured, the initial conditions have been assigned, the integration of the differential equation from t to t+Tp has been performed and, at the end, the predicted output and the predicted state has been obtained.

An important observation about NMPC controller is that the predicted output depends on the predicted state which depends on the command u(t).

The matrix Q, R, and P are the weighting matrices, and they must be well set for the correct functioning of the NMPC in order to give priority to the elements that must be minimized. In particular, the higher is the weight given to an element of the diagonal element of these matrices, more that signal is minimized. To be more precise, Q weights the state, R weights the inputs and P weights the terminal state (the state that corresponds to the last time instant of the prediction horizon). Q affects the weights of the state from the first discrete time instant to the one prior to the prediction horizon, P weights the state corresponding to the last time instant of the prediction horizon.

Matrices Q, R and P are diagonal matrices with non-negative elements. In particular, is important to outline that rank(Q)=n and rank(R)=m, where n is the system order and m is the number of input's variables.

The main drawback is that, increasing the prediction horizon, there is an exponential increasing of the number of region so there is a general slowdown of

the computational capabilities, for this reason is necessary a trade-off between performance and complexity of the closed loop control system.

3.3 Simplified and linearized system

Before to start with the control design, is necessary to check the controllability of the system.

Since the rank of the system is equal to the order of the simplified system (n=12), it is controllable and is possible to apply the NMPC controller on the whole state because rotations and translation have been considered coupled.

In this part of the work the system used is a linearized and simplified one, and for simplicity also the system used from the controller has a linear and simplified plant. The prediction model is equal to the plant.

The initial state given to the whole system, at the start, has been x0=[0 0 0 0 0 0 0 0 -50 0 0 0]^T , in order to consider the lasts 50 meters that separate the chaser from the target considering the Z axis.

The reference has been set to 0 in order to obtain the tracking of all the signals. In this phase the ‘’trial and error’’ procedure has been adopted.

The main difficulty in this phase is to choose the best values of Prediction horizon, Sampling time, and the weighting matrices R, Q and P, in order to obtain the best performance, to avoid wasting of computational power and of propellant.
In general, it results to be a good trade-off between tracking performance and speed of convergence.

The elements of R matrix have been chosen extremely close to zero because they must be different from zero due to intrinsic requirements of the MPC formulation.
In order to exploit all the available actuation (that in this phase of the maneuver is a key element) and to drive all the computational effort towards the optimization of the states, R matrix must be positive definite.

In the following table is possible to observe all the values of the parameters that give rise to the best tracking of the reference signal:

Parameter	**Chosen value**
Ts	0.05 s
Tp	0.7 s
Q	$\begin{bmatrix} 1 & 0 & 0 & 0 & 0 & 0 & 0 & 0 & 0 & 0 & 0 & 0 \\ 0 & 400 & 0 & 0 & 0 & 0 & 0 & 0 & 0 & 0 & 0 & 0 \\ 0 & 0 & 10 & 0 & 0 & 0 & 0 & 0 & 0 & 0 & 0 & 0 \\ 0 & 0 & 0 & 5 & 0 & 0 & 0 & 0 & 0 & 0 & 0 & 0 \\ 0 & 0 & 0 & 0 & 10 & 0 & 0 & 0 & 0 & 0 & 0 & 0 \\ 0 & 0 & 0 & 0 & 0 & 10 & 0 & 0 & 0 & 0 & 0 & 0 \\ 0 & 0 & 0 & 0 & 0 & 0 & 50 & 0 & 0 & 0 & 0 & 0 \\ 0 & 0 & 0 & 0 & 0 & 0 & 0 & 50 & 0 & 0 & 0 & 0 \\ 0 & 0 & 0 & 0 & 0 & 0 & 0 & 0 & 2 & 0 & 0 & 0 \\ 0 & 0 & 0 & 0 & 0 & 0 & 0 & 0 & 0 & 10 & 0 & 0 \\ 0 & 0 & 0 & 0 & 0 & 0 & 0 & 0 & 0 & 0 & 10 & 0 \\ 0 & 0 & 0 & 0 & 0 & 0 & 0 & 0 & 0 & 0 & 0 & 10 \end{bmatrix}$

P	$\begin{bmatrix} 100 & 0 & 0 & 0 & 0 & 0 & 0 & 0 & 0 & 0 & 0 & 0 \\ 0 & 1000 & 0 & 0 & 0 & 0 & 0 & 0 & 0 & 0 & 0 & 0 \\ 0 & 0 & 30 & 0 & 0 & 0 & 0 & 0 & 0 & 0 & 0 & 0 \\ 0 & 0 & 0 & 100 & 0 & 0 & 0 & 0 & 0 & 0 & 0 & 0 \\ 0 & 0 & 0 & 0 & 100 & 0 & 0 & 0 & 0 & 0 & 0 & 0 \\ 0 & 0 & 0 & 0 & 0 & 100 & 0 & 0 & 0 & 0 & 0 & 0 \\ 0 & 0 & 0 & 0 & 0 & 0 & 50 & 0 & 0 & 0 & 0 & 0 \\ 0 & 0 & 0 & 0 & 0 & 0 & 0 & 0 & 0 & 0 & 0 & 0 \\ 0 & 0 & 0 & 0 & 0 & 0 & 0 & 0 & 30 & 0 & 0 & 0 \\ 0 & 0 & 0 & 0 & 0 & 0 & 0 & 0 & 0 & 10 & 0 & 0 \\ 0 & 0 & 0 & 0 & 0 & 0 & 0 & 0 & 0 & 0 & 10 & 0 \\ 0 & 0 & 0 & 0 & 0 & 0 & 0 & 0 & 0 & 0 & 0 & 1300 \end{bmatrix}$
R	$\begin{bmatrix} 1\mathrm{e}-50 & 0 & 0 & 0 & 0 & 0 \\ 0 & 1\mathrm{e}-50 & 0 & 0 & 0 & 0 \\ 0 & 0 & 1\mathrm{e}-50 & 0 & 0 & 0 \\ 0 & 0 & 0 & 1\mathrm{e}-50 & 0 & 0 \\ 0 & 0 & 0 & 0 & 1\mathrm{e}-50 & 0 \\ 0 & 0 & 0 & 0 & 0 & 1\mathrm{e}-50 \end{bmatrix}$
tolerance	$[1e-3 \;\; 1e-3 \;\; 1e-3 \;\; 1e-3 \;\; 1e-3 \;\; 1e-3 \;\; 1e-3 \;\; 1e-3 \;\; 1e-3 \;\; 1e-3 \;\; 1e-3 \;\; 1e-3]'$
u_{min}	$[-0.7 \quad -0.7 \quad -0.7 \quad -0.7 \quad -0.7 \quad -0.7]$

u_{max}	$[0.7 \quad 0.7 \quad 0.7 \quad 0.7 \quad 0.7 \quad 0.7]$

Table 2 – First NMPC tuning (linearized system)

At the start the input saturation has been relaxed because having too strict saturations can bring to the destabilization of the system.

Relatively to the input actions, in correspondence of the peak control action, there is the highest value of the relative velocity that the chaser reaches with the impulsive maneuver.

Furthermore, to avoid overshoot on the X coordinate of the relative position, P matrix has been augmented with respect to Q matrix, and the prediction horizon has been increased.

In this section, an ideal scenario has been considered.

In particular, the disturbance acting on the satellite have been put almost to 0, and the considered system has been simplified.

In the following, is possible to see the overall results in terms of relative attitude between the docking port and the docking mechanism, the relative angular velocity, the relative P2P position between F_{dt} and F_{dt} and the relative P2P velocity.

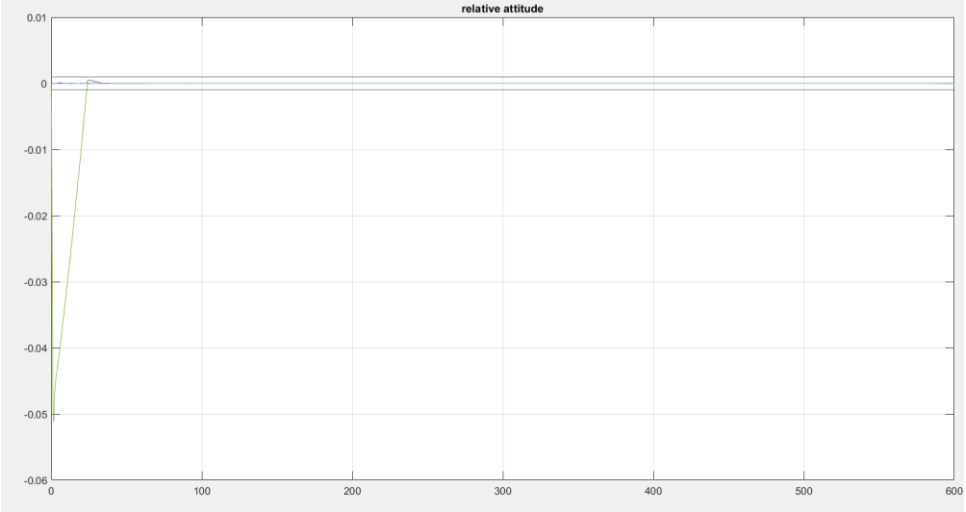

Figure 16 - Relative Attitude

Is possible to note that the y coordinate of the relative attitude has an undershoot that reaches -0.051 rad that corresponds to 2.92 degree, that is the expected result.

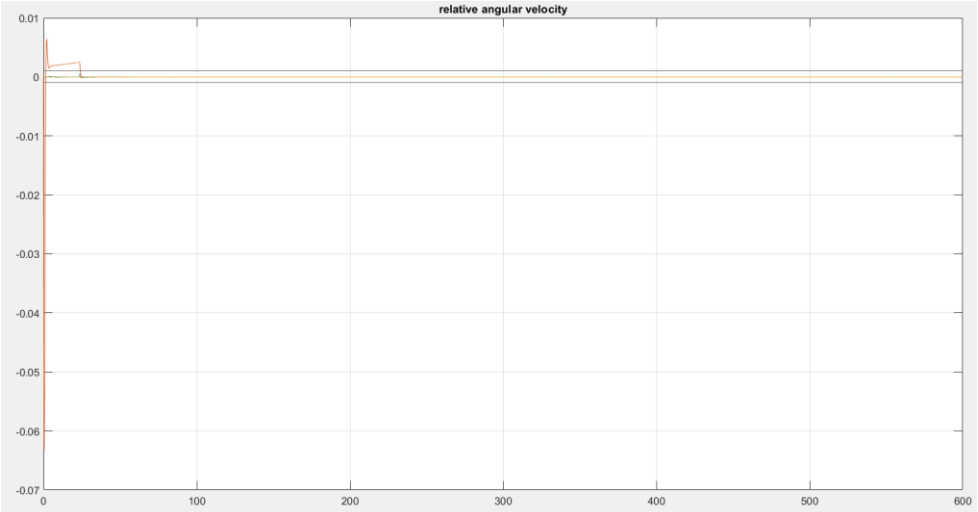

Figure 17 - Relative angular velocity

In the previous figure, is possible to see that the angular velocity has an undershoot that reaches -0.063 rad/s that corresponds to 3.6 degree/s and an overshoot on the y coordinate that reaches 6.44e-3 rad/s that is to say 1.6 degree/s, that is the expected result.

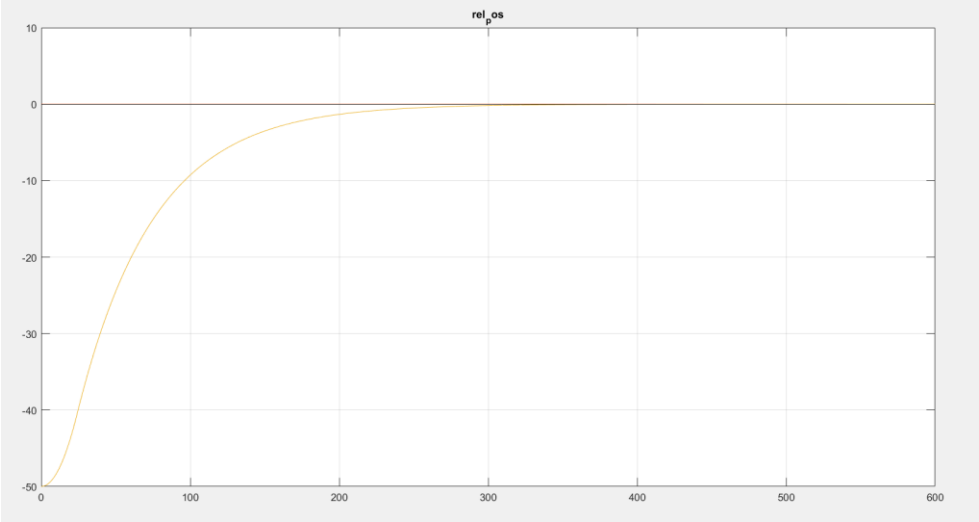

Figure 18 - Relative position

In the previous figure the tracking of the reference has been obtained, at the specified tolerance, after 571 s starting from a relative distance between the chaser and the target of 50 m. Furthermore, the lateral alignment of less than 0.01 m is respected.

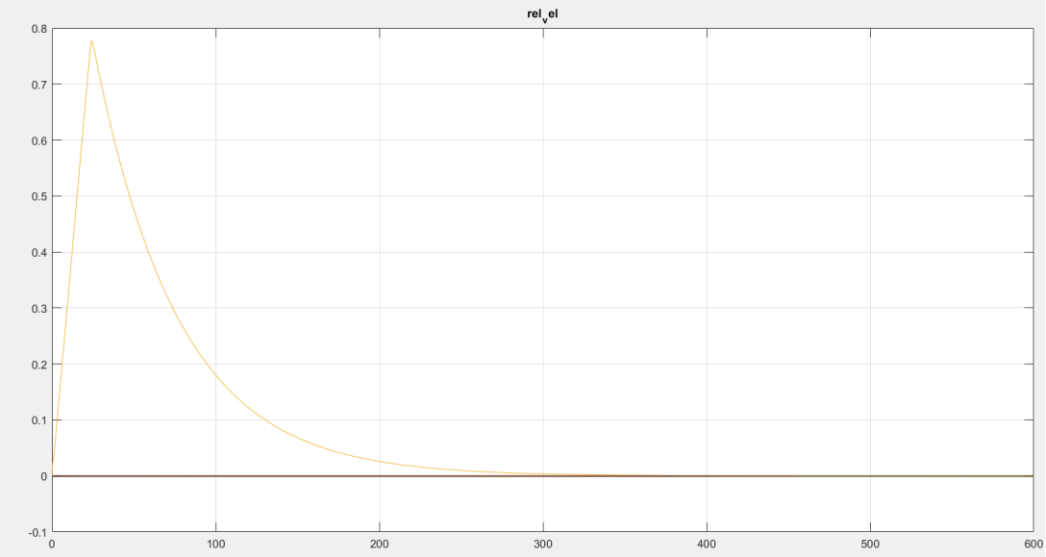

Figure 19 - Relative velocity

In the above figure, the max velocity reached is of 0.77 m/s and the convergence of the reference has been reached after 367 s with a millimeter speed. After the initial high velocity, it is deeply reduced. A better result would be obtaining a maximum speed of the max 0.3 m/s in order to have a not to high initial velocity.

In any case, the approach velocity at contact of less than 0.02 m/ and the lateral velocity of less than 0.01 m/s is respected at the end of docking;

The choice of a smaller prediction horizon improves the overall performance of the system at the expense of a slower response of it, that, in this case, where the purpose is a soft docking, is not considered as a drawback because if a suitable tradeoff is found between speed of the system and satisfaction of constraints, a slower system is easier to handle. Choosing a smaller value of prediction horizon reduces the number of regions of the optimizing polytope, and this reduces the computation time. Increasing the prediction horizon, larger values of final

relative position and velocity are obtained due to numerical conflict for the complexity of the optimization problem.

3.4 Simplified and not linearized system

At this moment is necessary to consider also the non-idealities of the system.

Previously the system has been linearized around specific equilibrium points.

Now, instead, the main difficulties is considering all the non-linearities.

It must be kept in mind that between the linearized and the non-linearized plant there are the linearization's errors.

In this part of the project has been considered the nonlinear plant, using a Matlab function that can be found in the Appendix 2, with all equations obtained in the chapters 2.1 and 2.2 and a linear MPC controller.

To do a step at a time, has been decided to use the nonlinear, but simplified model considering as state variable only the relative attitude and angular velocity, relative position and velocity.

The classic approach would have been using a nonlinear controller due to the fact that the plant is nonlinear. This solution would have been also more intensive in terms of computation complexity. In the next subchapter, this argument will be deal with.

In this subchapter, instead, the linear MPC design theory combined with the nonlinear and simplified plant have been used.

Using a linear MPC controller applied to a nonlinear plant is a technique that has been found also in [12] but using the Artificial Neural Network (ANN). The control model has been used to predict a process behavior over the horizon of interest.

Since lot of plants shows a nonlinear behavior, using nonlinear MPC would be a difficult task. In this article is presented a Neural Network based model predictive control strategy, that involves a nonlinear plant modeling with ANN.

In this part of the work, values that represent disturbances have been added, but they are not the real ones; anyway also the variables suffers the effects of them.

In general disturbance's torques on attitude are very small and so they have been put to values near to 0.

There is the aerodynamic torque that in general is of the order of 10^{-10}, solar pressure that is almost absent and gravitational pressure that must be calculated every time the position in the orbit changes. For simplification they have been put to 10^{-10}, but they have been added to make the problem more realistic.

In the next figure is possible to observe the Simulink model used for the simulation: the nonlinear plant has been built with the Simulink Function block, where the arguments are the state x and the inputs u, the output of the function has been integrated and is became the input of the function itself. The final output of the system (the state) was the input, together with the reference to track, of the NMPC block.

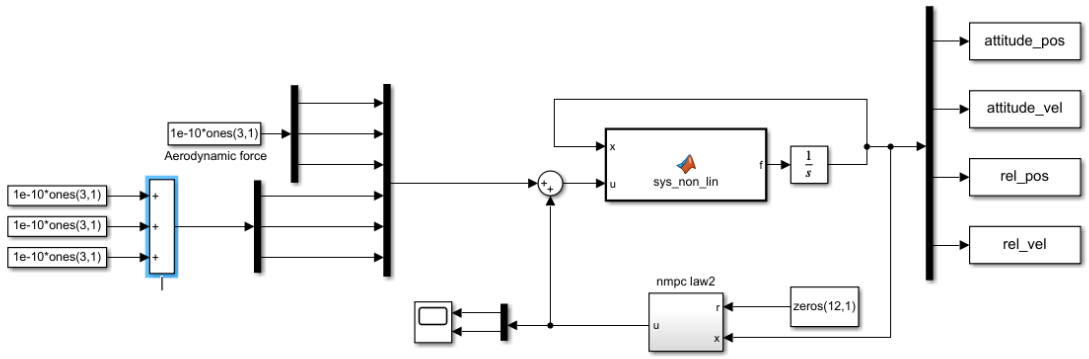

Figure 20- Simulink Model (Nonlinear plant)

The model used for the controlling task is the linearized model.

The way to do the tuning on nmpc parameter is increasing of one order of magnitude each parameter of the weighting matrices once a time until a good trade-off between tracking performance, speed of convergence and maximum overshoot is obtained.
The elements of R matrix have been chosen extremely close to zero because they must be different from zero due to intrinsic requirements of the MPC formulation and, as has been already said, R matrix must be positive definite.

In the following table is possible to observe all the values of the parameters that give rise to the best tracking of the reference signal:

Parameter	Chosen value
Ts	0.05 s
Tp	0.58 s
Q	$\begin{bmatrix} 500 & 0 & 0 & 0 & 0 & 0 & 0 & 0 & 0 & 0 & 0 & 0 \\ 0 & 1000 & 0 & 0 & 0 & 0 & 0 & 0 & 0 & 0 & 0 & 0 \\ 0 & 0 & 100 & 0 & 0 & 0 & 0 & 0 & 0 & 0 & 0 & 0 \\ 0 & 0 & 0 & 500 & 0 & 0 & 0 & 0 & 0 & 0 & 0 & 0 \\ 0 & 0 & 0 & 0 & 1000 & 0 & 0 & 0 & 0 & 0 & 0 & 0 \\ 0 & 0 & 0 & 0 & 0 & 100 & 0 & 0 & 0 & 0 & 0 & 0 \\ 0 & 0 & 0 & 0 & 0 & 0 & 420 & 0 & 0 & 0 & 0 & 0 \\ 0 & 0 & 0 & 0 & 0 & 0 & 0 & 50 & 0 & 0 & 0 & 0 \\ 0 & 0 & 0 & 0 & 0 & 0 & 0 & 0 & 20 & 0 & 0 & 0 \\ 0 & 0 & 0 & 0 & 0 & 0 & 0 & 0 & 0 & 10500 & 0 & 0 \\ 0 & 0 & 0 & 0 & 0 & 0 & 0 & 0 & 0 & 0 & 300 & 0 \\ 0 & 0 & 0 & 0 & 0 & 0 & 0 & 0 & 0 & 0 & 0 & 100 \end{bmatrix}$
P	$\begin{bmatrix} 100 & 0 & 0 & 0 & 0 & 0 & 0 & 0 & 0 & 0 & 0 & 0 \\ 0 & 1000 & 0 & 0 & 0 & 0 & 0 & 0 & 0 & 0 & 0 & 0 \\ 0 & 0 & 800 & 0 & 0 & 0 & 0 & 0 & 0 & 0 & 0 & 0 \\ 0 & 0 & 0 & 100 & 0 & 0 & 0 & 0 & 0 & 0 & 0 & 0 \\ 0 & 0 & 0 & 0 & 100 & 0 & 0 & 0 & 0 & 0 & 0 & 0 \\ 0 & 0 & 0 & 0 & 0 & 100 & 0 & 0 & 0 & 0 & 0 & 0 \\ 0 & 0 & 0 & 0 & 0 & 0 & 9000 & 0 & 0 & 0 & 0 & 0 \\ 0 & 0 & 0 & 0 & 0 & 0 & 0 & 10 & 0 & 0 & 0 & 0 \\ 0 & 0 & 0 & 0 & 0 & 0 & 0 & 0 & 300 & 0 & 0 & 0 \\ 0 & 0 & 0 & 0 & 0 & 0 & 0 & 0 & 0 & 60000 & 0 & 0 \\ 0 & 0 & 0 & 0 & 0 & 0 & 0 & 0 & 0 & 0 & 100 & 0 \\ 0 & 0 & 0 & 0 & 0 & 0 & 0 & 0 & 0 & 0 & 0 & 3000 \end{bmatrix}$

R	$\begin{bmatrix} 1e-50 & 0 & 0 & 0 & 0 & 0 \\ 0 & 1e-50 & 0 & 0 & 0 & 0 \\ 0 & 0 & 1e-50 & 0 & 0 & 0 \\ 0 & 0 & 0 & 1e-50 & 0 & 0 \\ 0 & 0 & 0 & 0 & 1e-50 & 0 \\ 0 & 0 & 0 & 0 & 0 & 1e-50 \end{bmatrix}$
tolerance	$[1e-3 \;\; 1e-3 \;\; 1e-3 \;\; 1e-3 \;\; 1e-3 \;\; 1e-3 \;\; 1e-3 \;\; 1e-3 \;\; 1e-3 \;\; 1e-3 \;\; 1e-3 \;\; 1e-3]'$
u_{min}	$[-0.7 \;\; -0.7 \;\; -0.7 \;\; -0.7 \;\; -0.7 \;\; -0.7]$
u_{max}	$[0.7 \;\; 0.7 \;\; 0.7 \;\; 0.7 \;\; 0.7 \;\; 0.7]$

Table 3 - Second NMPC tuning (Nonlinear system)

The used initial condition has been: x0=[0 0 0 0 0 0 -50 0 0 0 0 0]' , so considering 50 meters that separates the chaser from the target on the x coordinate of the relative position (V-bar approach).

During the 'trial and error' nmpc tuning has been noted that increasing the Prediction Horizon Tp has two effects: the positive one was that a tracking that fulfilled the requirement was obtained for how much concern the relative

position, but the drawback was that the maximum peak of the relative velocity has been increased.
At the same time, increasing the x coordinate of the velocity in the Q matrix reduced the maximum peak of the velocity but had the drawback that the tracking of the x coordinate of the position to the reference (respecting the requirements) was not obtained.
Another effect that has been noted was that increasing the x coordinate of the position of the Q matrix the tracking improved.

In the following figure is possible finding the best results obtained by the 'trial and error' tuning:

In the following figure is shown the relative attitude between the chaser and the target represented in rad. Is possible to observe the noises probably due to the disturbances added to the system due to numeric errors. The initial condition considered is, in this case [0; 0; 0] rad that means 0 degrees, so in this case has been considered that at the start there is no rotation between the two spacecrafts.

As seen in *Figure 22*, the maximum value reached from the x coordinate of the relative attitude is almost 0.005 rad, that corresponds to 0.28 degrees. This result is conformed to the requirements on the attitude for which the max value that the relative attitude, at contact, should be less than 1 degree.

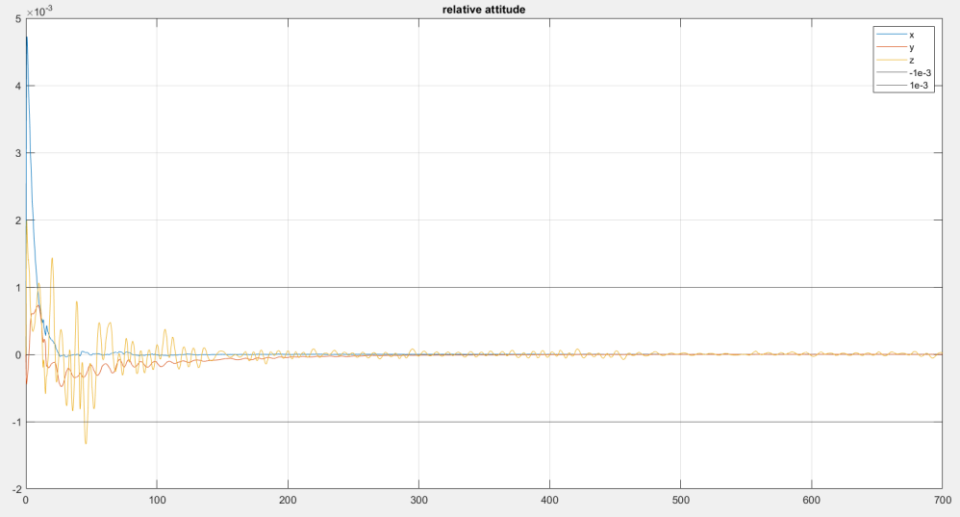

Figure 21 - Relative attitude

In the following figure, the relative angular velocity between the chaser and the target is represented in rad/s. Also here is possible to find some noises in the representation of the three axes and are valid the same consideration of the previous case. The initial condition considered is, in this case [0; 0; 0] rad that means 0 degrees. The maximum value reached at contact is less then 0.1 deg/s, so it is conformed to the requirements.

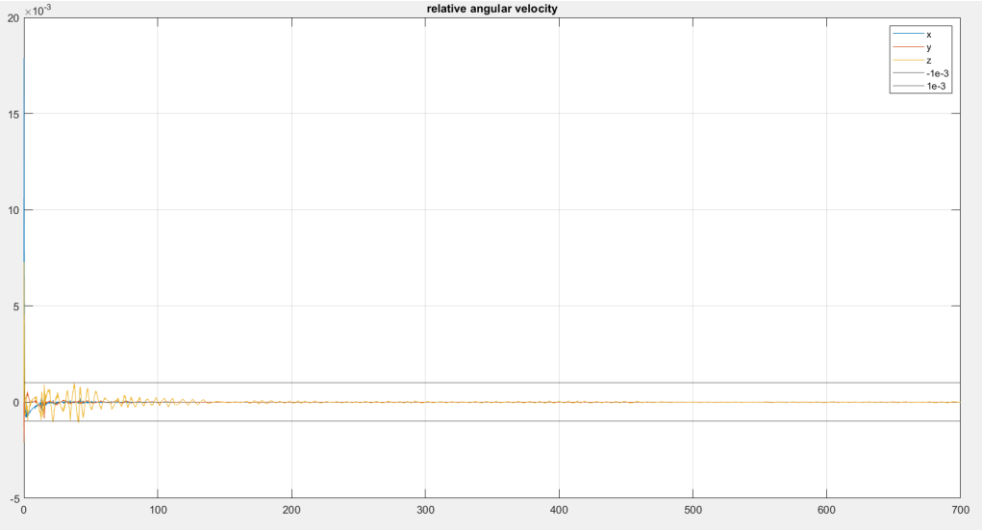

Figure 22 - Relative Angular Velocity

In the following figure is shown the relative position between the two spacecrafts and it is represented in meters. In this case the initial conditions considered was [-50; 0; 0]. As told in the chapter 1, the requirements in term of position were having lateral alignment at docking (lateral means not respect to the docking axis that is x axis, but with respect the y and z axis) less then 0.01 m. The previous requirement is respected, and the tracking is obtained avoiding overshoots on the x coordinates.

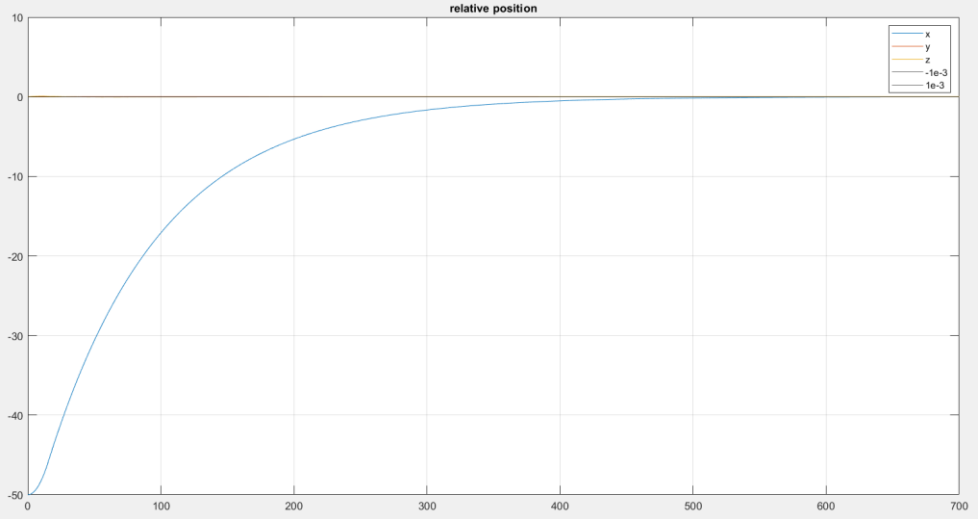

Figure 23 - Relative Position

In the following figure is shown the relative velocity between the two spacecrafts and is represented in m/s. In this case the initial conditions considered was [0; 0; 0]. The requirements in term of velocity were having lateral velocity less then 0.01 m/s and approach velocity (along the docking axis) less then 0.02 m/s. The previous requirement is respected, and the tracking is obtained.

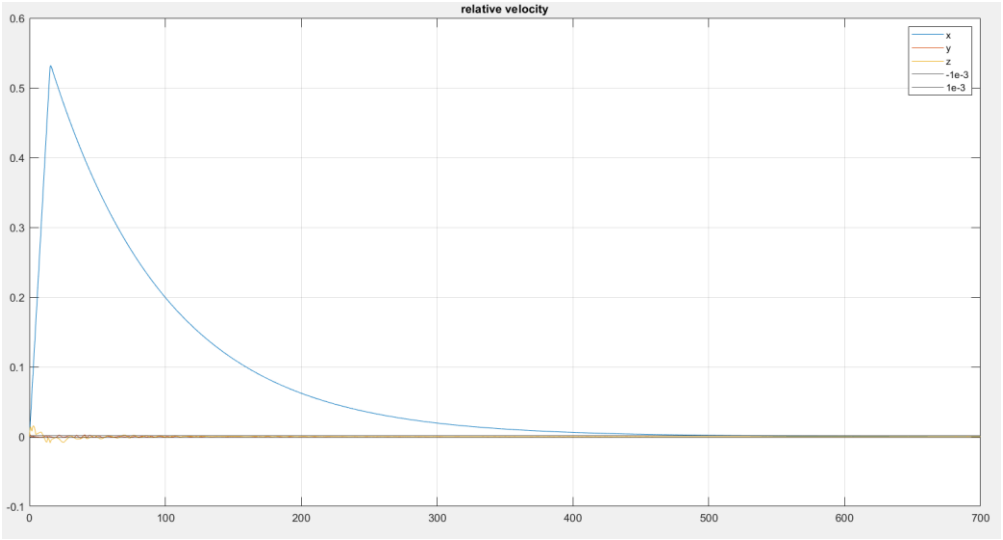

Figure 24 - Relative Velocity

The next two figures report the control effort along the three axes.

In the following, is possible to observe the behavior of the first input considered that is Tdc (the docking chaser torque). The upper and lower bounds, in the control law, have been fixed to 0.7 and -0.7, and is possible to note that, after the first seconds of oscillations, the behavior settles to the reference. Furthermore, the maximum level of thrust is not reached.

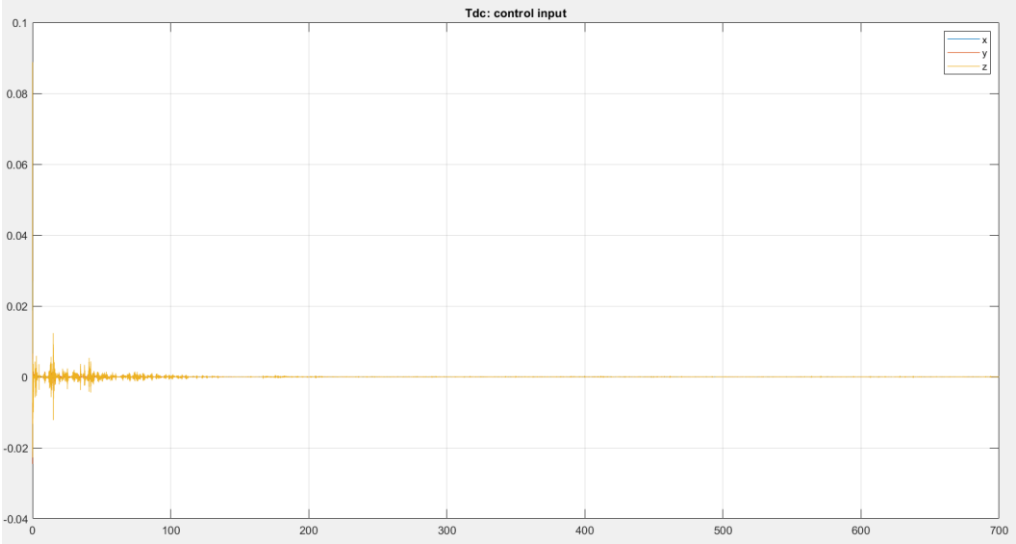

Figure 25 - Tdc (control input)

In the next figure is represented the behavior of the first input considered which is Fdc (the docking chaser force). The consideration made for the previous case are still valid.

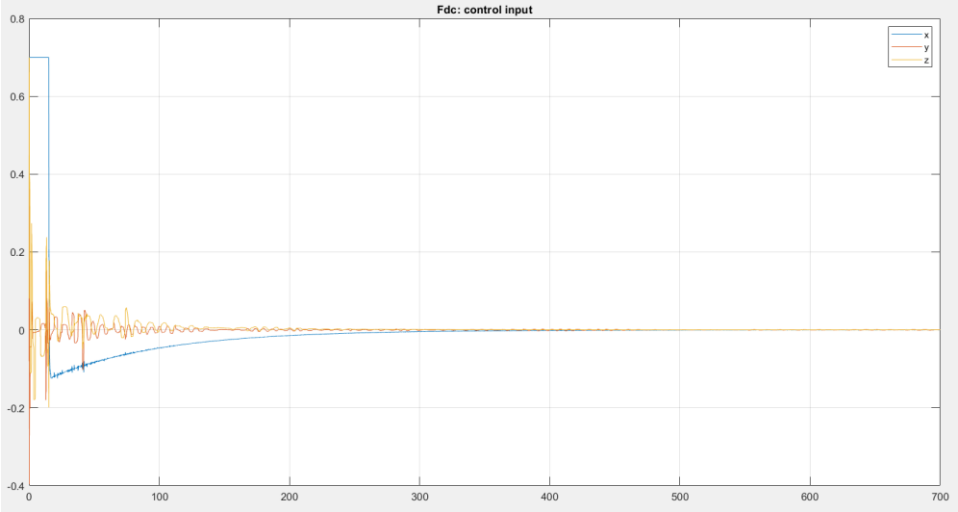

Figure 26 - Fdc (control input)

Reducing the saturation constraint on the control input from 0.7 for the upper bound and -0.7 for the lower bound, to 0.3 and -0.3, results in a faster tracking of the reference signal and a total accomplishment of the requirements. Is important to note that the less is the saturation constraint, the less is the effort that the propulsor has to do and the less is the control effort and the propellant consumption, and the less is the effort from the point of the reaction wheels, the less is the effort of electric power.

3.4.1 Increasing the Prediction Horizon

Increasing the Prediction Horizon Tp to 0.8 s yelds to similar results:

As regards the angular velocity there will be more noises, but the requirements are fulfilled because the value that those coordinates can reach at contact is less than 1 degree:

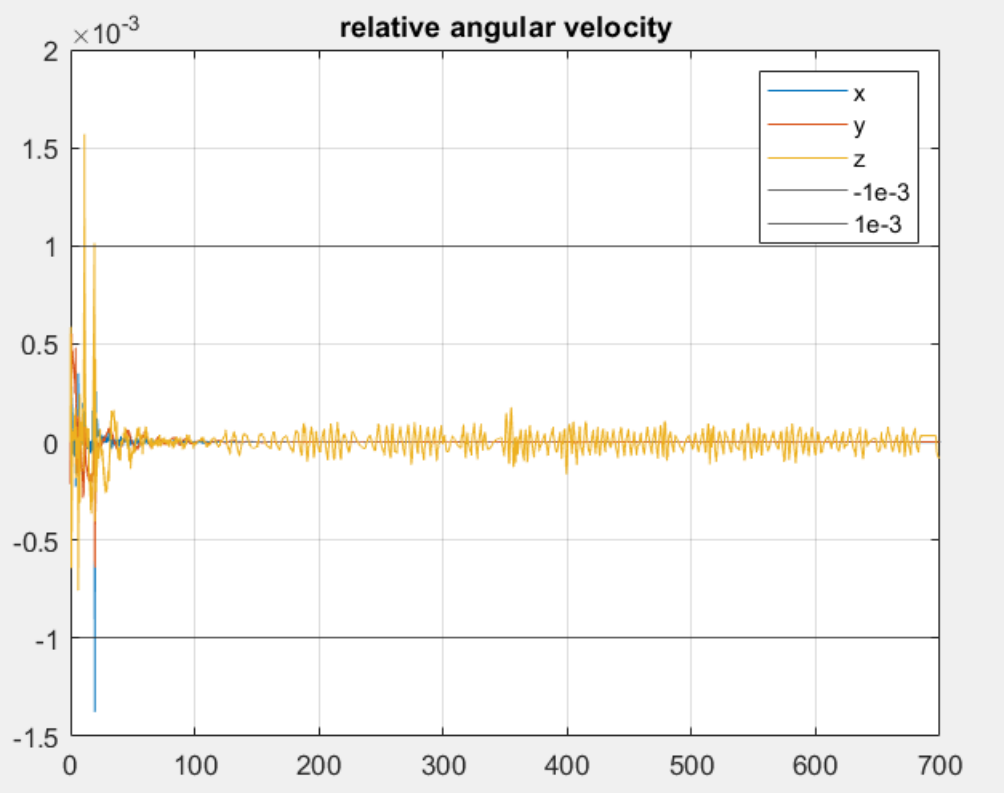

Figure 27 - Relative Angular Velocity

The same consideration of before is valid also for the relative attitude because the value that those coordinates can reach at contact is less than 0.1 deg/s:

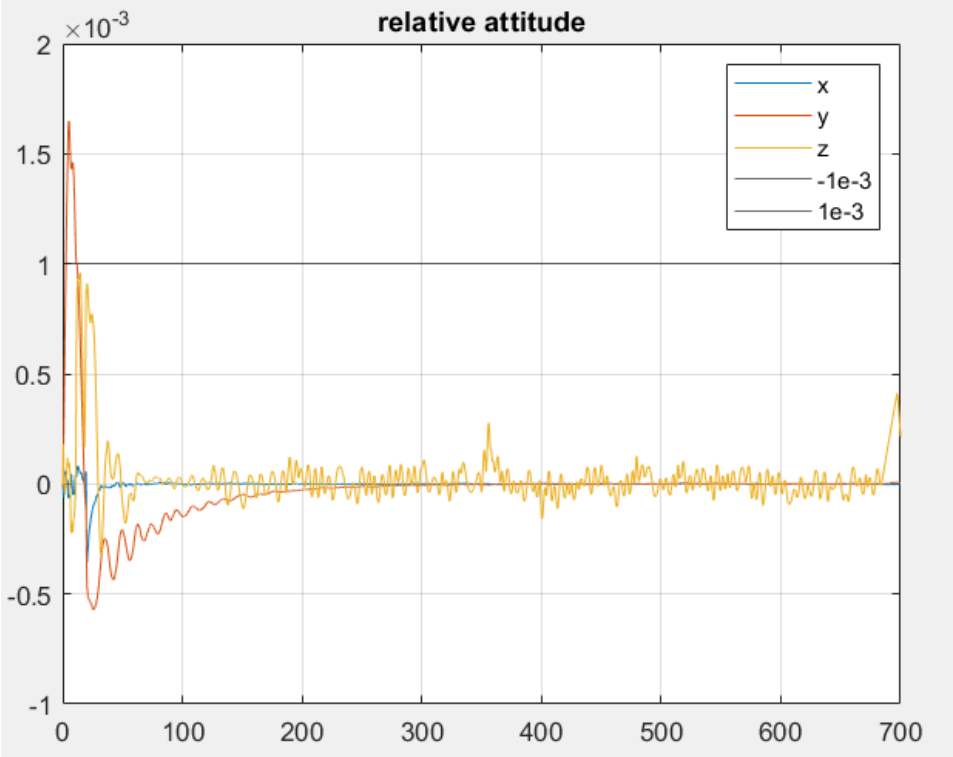

Figure 28 - Relative Attitude

Regarding the relative position the tracking of the reference happens in less than 500 s, so is faster than the previous case, in this way the mating phase is reached before.

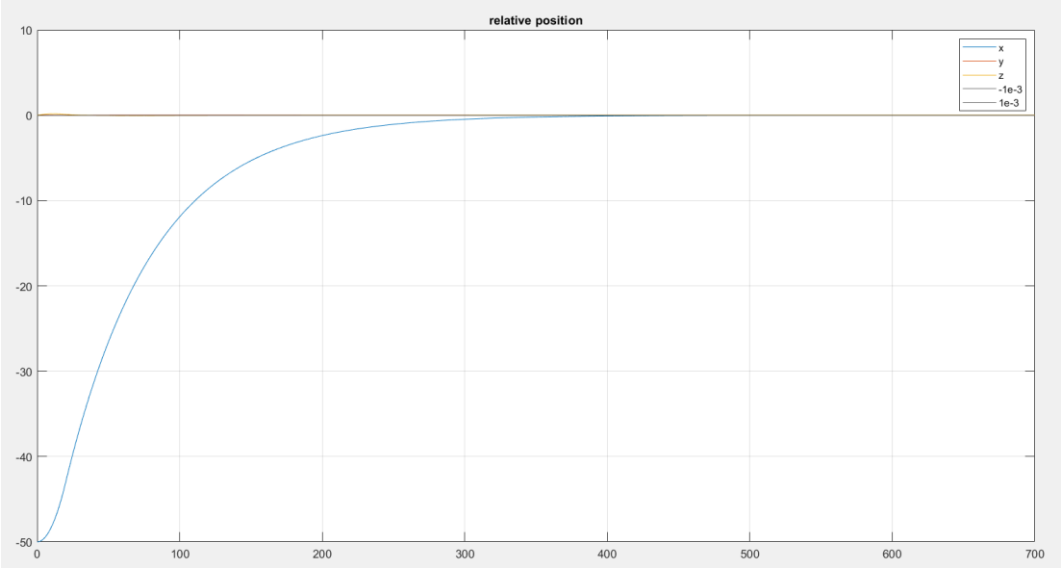

Figure 29 - Relative Position

The relative velocity has a higher peak on the approach axis, it almost arrives at 0.7 m/s, but the tracking of the reference is faster. Furthermore, the approach velocity at contact of less than 0.02 m/s and the lateral velocity of less than 0.01 m/s is respected at the end of docking;

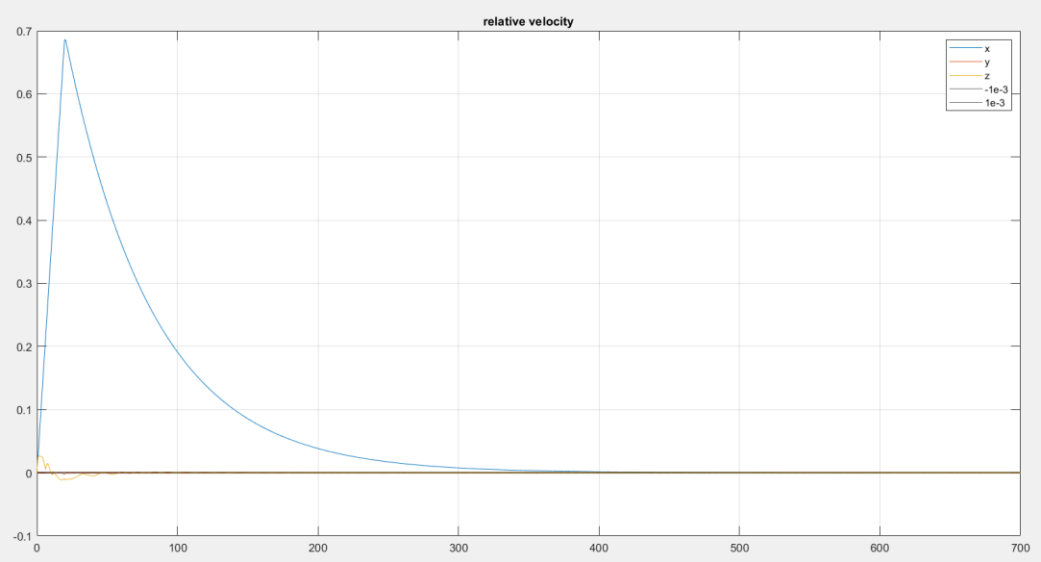

Figure 30 – Relative velocity

Inside the NMPC block a STOP Simulation has been added in order to interrupt the simulation when the chaser arrives almost to reach the 0 meters on the approach axis or 1 mm of distance from the target, in order to have the capture between the two spacecrafts. In order to do so, has been used the Simulink's signal of stop where there is a function that receives as input the value of the x position (approach axis). In this way the simulation will be stopped when the capture is almost reached.

4. Disturbances

A variety of source in space cause disturbance forces and torques that act on a body in space. These forces/torques are categorized as *cyclic*, varying in a sinusoidal manner during an orbit, or *secular*, accumulating with time.

Unless resisted in some way, the torques would reorient the vehicle, while the forces would let the trajectory change.

The control system acts in 2 ways:

1. Actively by sensing the resulting motion and applying corrective forces or torques.
2. Passively by exploiting the inertia or magnetic properties to make the disturbances stabilizing and their effect tolerable.

Is known that disturbance sources can be:

- Atmospheric drag
- Gravity-gradient
- Solar radiation pressure
- Planet's magnetic field
- Orbital perturbations

There can be other disturbances that may arise from the internal of the spacecraft when some parameters are uncertain. In the next chapter this case will be analyze and will be explained that to have control over them, they must be considered in the project and designed accordingly or reducing their effects in order to meet the requirements.

In the first part of the project disturbances have not been considered, in the chapter 3.4 they have been added, but not considering the fact that they are not constant, and they vary in time and with the satellite's attitude. They are subject to formulas and constants.

In the following part of the work there will be the analysis of each single disturbance:

1. ***Aerodynamic drag***:

   Is known that a vehicle moving in the atmosphere is subject to drag In particular, the force due to the residual atmosphere reduces the velocity of the spacecraft, so it reduces the orbit size. Due to any offset that exists between the center of mass and the aerodynamic center of pressure (r_{cp}: vector in body coordinates), this drag force will produce a disturbance torque acting on the S/C.

   The aerodynamic torque is given by:

$$\overrightarrow{\mathrm{Ta}} = \overrightarrow{\mathrm{rcp}} \times \overrightarrow{\mathrm{Fa}}$$

Equation 11 - Aerodynamic Torque

Where:

$$\vec{F}_a = \frac{1}{2}\rho \cdot V^2 \cdot S \cdot C_D \cdot \frac{\vec{V}}{V}$$

ρ = atmosphere density

V = spacecraft velocity

S = spacecraft projected area normal to $\vec{V}$

C_D = drag coefficient

2. *Gravity-gradient*

According to the Newtonian $1/r^2$ law, the planetary gravitational field decrease with the distance r from the planet. For this reason, an object in orbit will have a stronger attraction on its lower side then on its upper side. Obviously, this differential attraction results in a torque tending to rotate the object to align its minimum inertia axis with the local vertical.

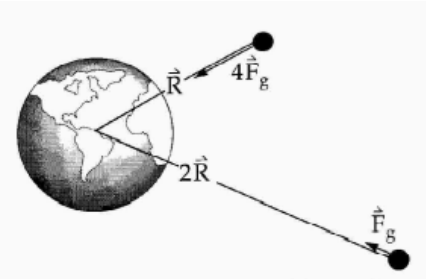

Figure 31

A restoring torque toward the stable vertical position is product by perturbations from this equilibrium and cause a periodic oscillatory motion.

The energy dissipation in the S/C will damp this motion.

The gravity-gradient torque T_g for a satellite in a near-circular orbit is:

$$\overrightarrow{Tg} = 3n^2\hat{r} \times [I]\hat{r}$$

Equation 12 - Gravity Gradient torque

Where:

$\hat{r} = \vec{r}/r$ = unity vector from planet to spacecraft

$n^2 = \mu/a^3 = \mu/R^3$ = orbital rate

μ = gravitational constant

I = spacecraft inertia matrix

3. *Radiation pressure*

Is known that solar radiation pressure can produce disturbance torque. The solar radiation pressure T_s is, in body coordinates:

$$\overrightarrow{Ts} = \overrightarrow{rsp} \times \overrightarrow{Fs}$$

Equation 13 – Solar Radiation Pressure

Where:

$\vec{r}_{sp}$ = vector from body centre of mass to spacecraft optical centre of pressure

$F_s = (1+K) \cdot p_s \cdot A_\perp$

K = spacecraft surface reflectivity, $0 < K < 1$

$A_\perp$ = spacecraft projected area normal to sun vector

$p_s = I_s/c$; $\quad I_s = 1370\, W/m^2$ @ 1 AU; $\quad c = 2.9979E8\, m/s$

This solar radiation torque is independent from the spacecraft's position or velocity and is perpendicular to the sun line. Instead, the aerodynamic torque is proportional to the atmospheric density. Above 1000-km altitude, solar radiation pressure usually dominates the spacecraft disturbance torque environment, but in this case has been considered to be at 500 Km of altitude, so this kind of disturbance will not be taken in consideration in the present work.

4. Magnetic field

Earth and other planets such as Jupiter that have a substantial magnetic field exert yet another torque on spacecraft in low orbits about the primary. The magnetic torque Tm on the spacecraft is given by:

$$\overrightarrow{\mathrm{Ts}} = \overrightarrow{\mathrm{M}} \times \overrightarrow{\mathrm{B}}$$

Equation 14 - Magnetic Torque

Where:

- M is the spacecraft dipole moment due to current loops and residual magnetization in the spacecraft [Am^2 per turns].
- B is the Earth magnetic field vector expressed in spacecraft coordinates, and measured in tesla [T]; its magnitude is proportional to the magnetic moment of the Earth (7.96E-15 Tm3) and to $1/r^3$, where r is the radius vector to the spacecraft.
- The magnetic torque on such a spacecraft in low orbit would then be approximately 3 x 10-6Nm.
- Magnetic torque may well be a disturbance torque. However, it is common to reverse the viewpoint and take advantage of the planetary magnetic field as a control torque to counter the effects of other disturbances.

4.1 Disturbances's addition to the Simulink Model

In this section will be analyzed the results of the simulation introducing all torques and forces in the previously used Simulink Model. All these torques and forces represent the disturbances that acts on the satellite.

The updated model will be:

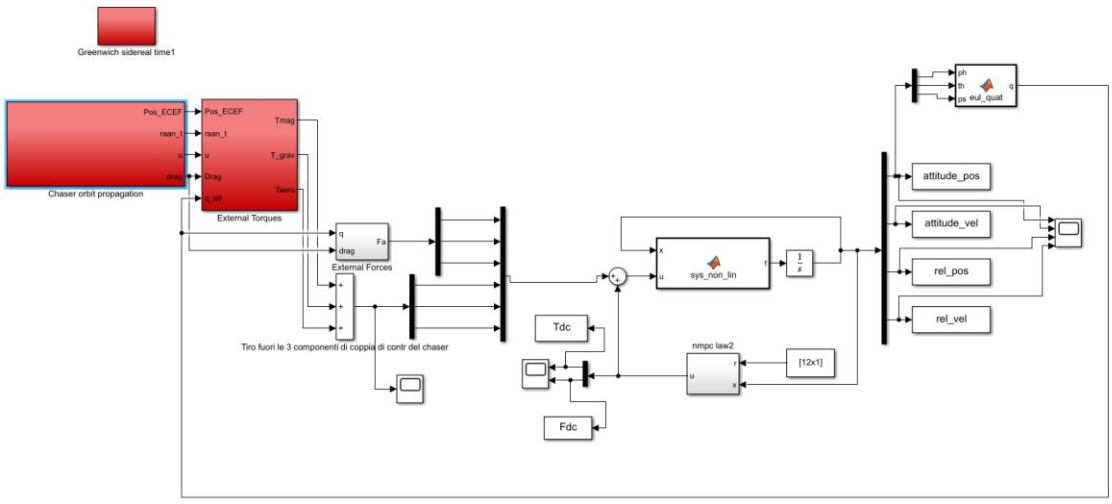

Figure 32 - Overall System including disturbances

On the right is possible observing a Simulink block where there is a Matlab Function that takes the Euler angles that represents the relative attitude position of the two spacecrafts and transforms them into quaternions through the "Elementary quaternions".

Inside the left red block 'Chaser orbit propagation' is possible to find some constant parameters used to calculate the disturbances. In particular, there are some specific Matlab functions that describe the Aerodynamic Resistance, the

orbital life and the Ephemeris computation such as the true anomaly, the correct RAAN (for geocentric orbit the longitude is also called right ascension of ascending node (RAAN)), the latitude and the punctual velocity. From the first red block, as output is possible to find the coordinates of the position in the Earth centered earth fixed (ECEF) frame, the aerodynamic drag, the correct RAAN, and the true anomaly (indicated with the letter u).

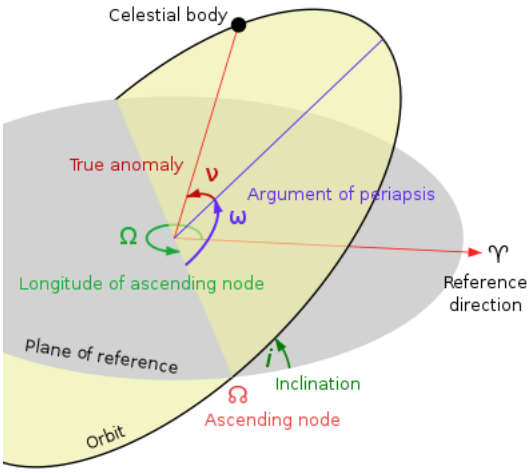

Figure 33 – Ephemeris computation

Those are the input to the second red block inside the one there is the effective computation of the considered disturbance torques. Inside this second red block is performed the magnetic field computation, the residual magnetic torque, the gravity gradient, and the aerodynamic drag torque using the formulas explained in the previous chapter.

All those torques and forces has been summed and has been put as inputs to the considered system. The sum of all disturbances torques, is, as expected of the order of 10^{-6}.

4.2 Simulation

Is possible to observe that, despite the addition of disturbing's torques and forces, the obtained results respect the requirements.

Adding those disturbances to the system and using the same NMPC parameter configuration of before (chapter 3.3.1), the following results has been obtained:

In the following figure, where the relative attitude is represented, there is less noise with respect to the previous case, but the requirements are fulfilled because the value that those coordinates can reach at contact is less than 1 degree.

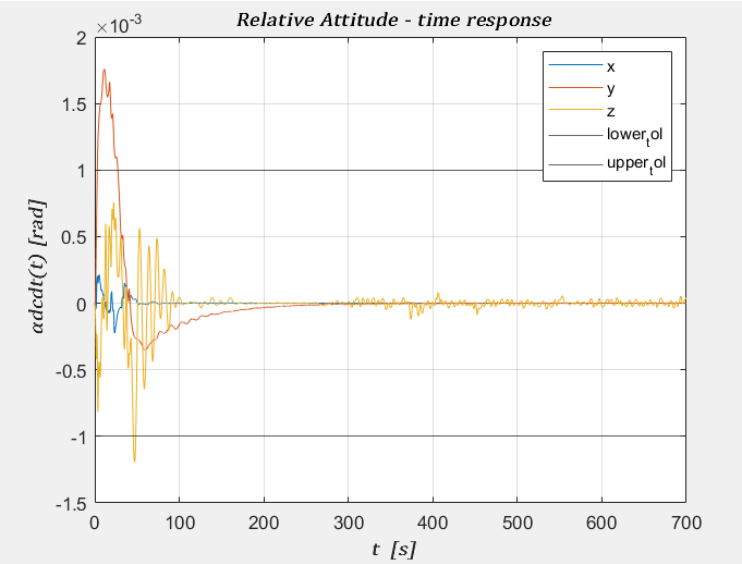

Figure 34 - Relative Attitude (with disturbances)

In the following figure, that represents the relative angular velocity, the max value that those coordinates can reach is less than 0.1 deg/s, in particular 0.0009 rad/s corresponds to 0.05 deg/s, for this reason the requirement at contact is

fulfilled. Furthermore, the highest peak is less than the previous case without disturbances:

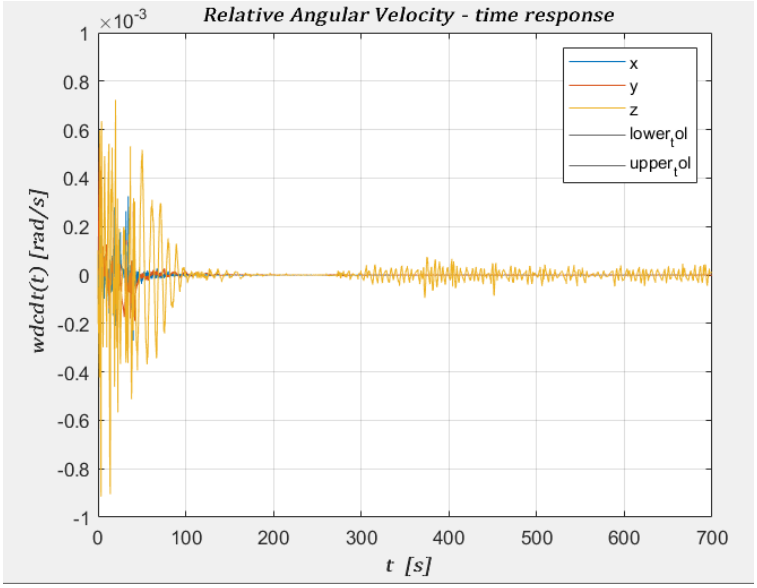

Figure 35 - Relative Angular Velocity (with disturbances)

In the following figure, the relative position between the chaser and the target has been simulated. After 210 s the lateral relative position (on the z coordinate) became less than 0.01 m (as expected from the requirements). After 697 s the relative position along the docking axis (x axis considering a V-bar approach) reaches the value of 0.001 m, that means 1 mm.

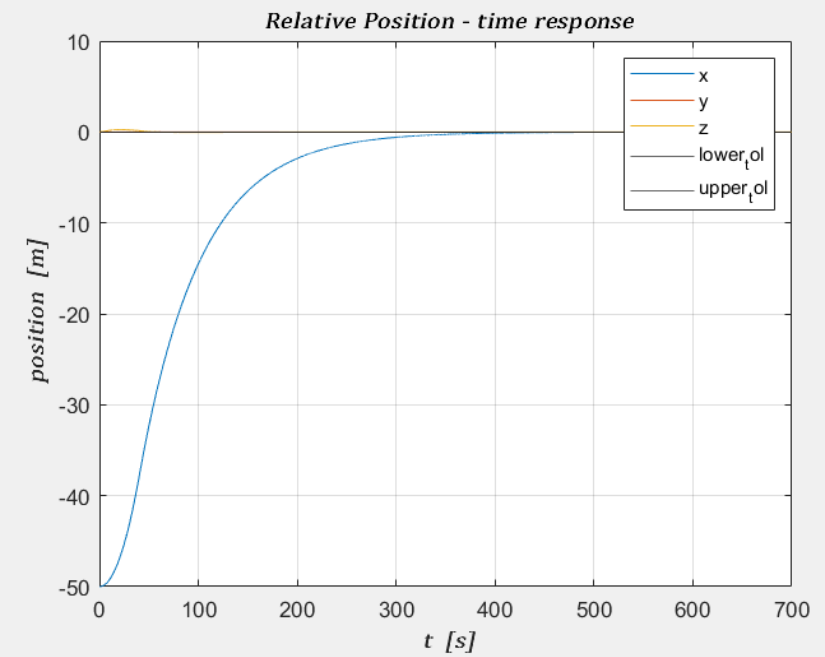

Figure 36 - Relative Position (with disturbances)

In the following figure is possible to observe that the lateral velocity is always less then 0.3 m/s. The approach velocity reaches the peak value of 0.6 m/s, but then rapidly decrease until reaching the value of 0.02 m/s after 250 s of simulation. After 440 s, the approach velocity reaches the value of 0.001 m/s, and it means that the approach velocity is of the order of the millimeter. It means that the cubeSat is arriving to the target always slower, the contact velocity cannot be 0 otherwise there wouldn't be the contact between the two spacecrafts.

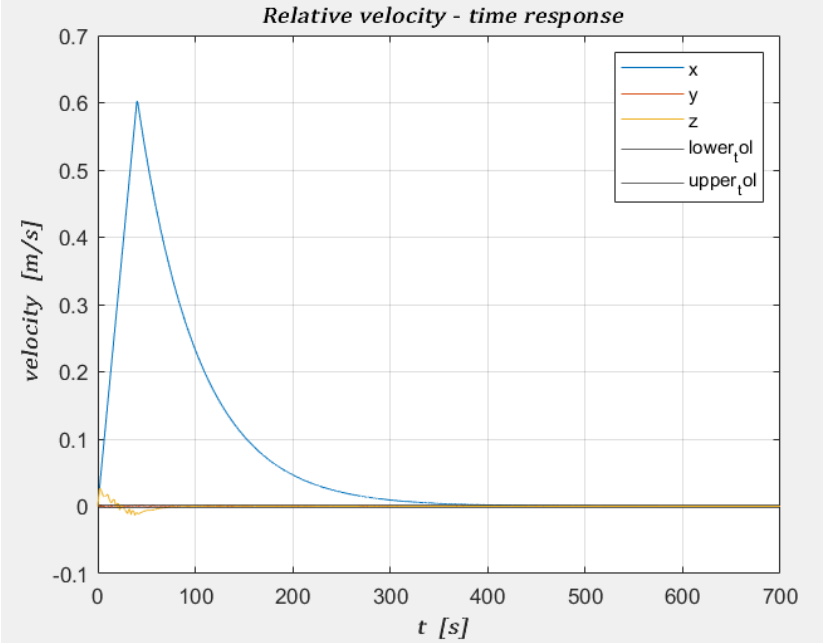

Figure 37 - Relative Velocity (with disturbances)

In the following figure are represented both the control inputs. Is possible to observe that the Fdc saturate to 0.3 due to the used constraints on the upper and lower bound of the input.

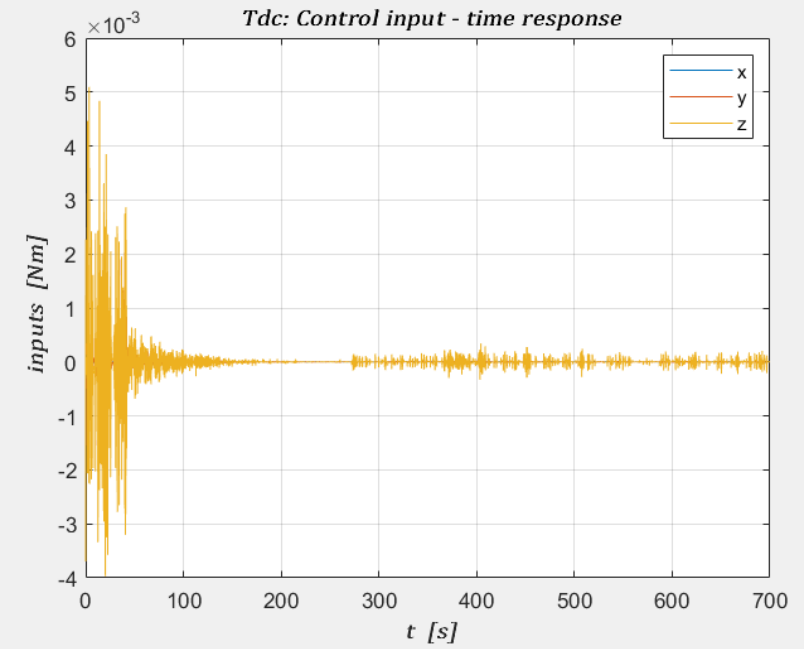

Figure 38 - Tdc: Control input (with disturbances)

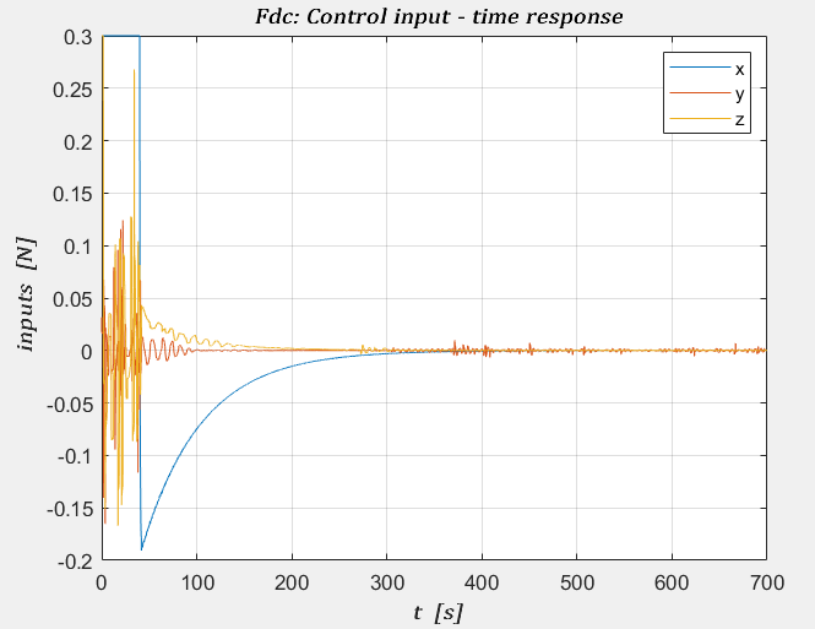

Figure 39 - Fdc: control input (with disturbances)

4.3 Parameter's perturbation

In the following section, has been considered the fact that the parameters of the intern model are different from the ones of the true system. For this reason, could be of interest controlling the robustness of the system varying the uncertain parameters and observing if the same controller used before, with the identical parameters, continue to work in a good way.

Is known that every uncertain parameter has a range of uncertainty. The following simulations have been performed varying of the 10% the chaser mass, the altitude of the orbit and the distance between the CoM of both the spacecraft and the docking port.

As is possible to see in the following simulations, the obtained results are still good, so it means that the system is robust. The only modifications that occur are a small increasing of the max value of one of the coordinates of the relative attitude (that arrives at 0.11 deg), a small increasing of the max value of one of the coordinates of the relative angular velocity (that arrives at 0.11 deg)

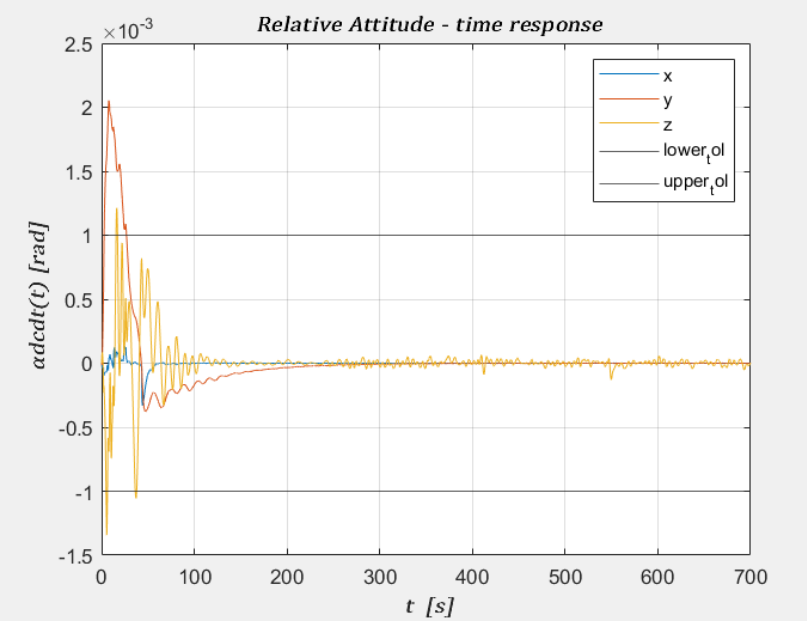

Figure 40 - Relative Attitude (parameter's perturbation)

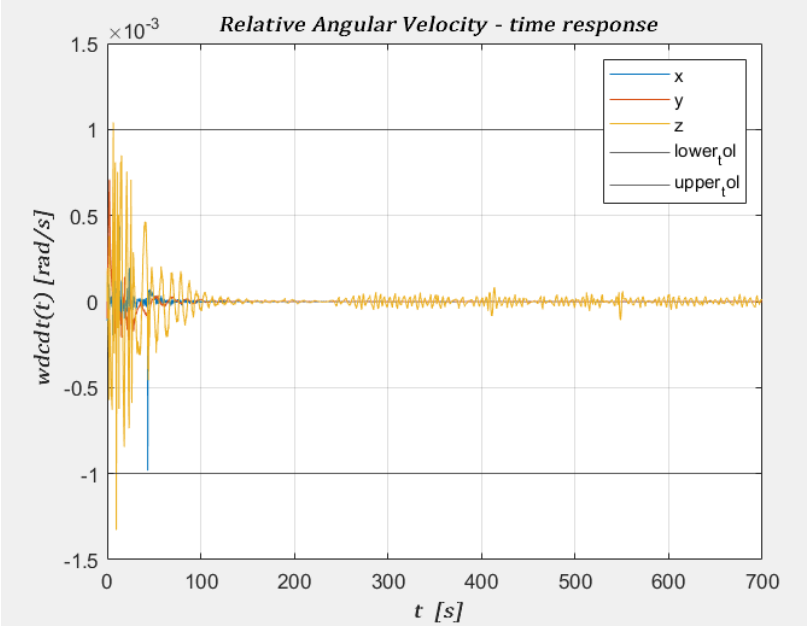

Figure 41 - Relative Angular Velocity (parameter's perturbation)

As seen in the following figure, after 698 s the relative position along the docking axis (x axis considering a V-bar approach) reaches the value of 0.001 m, that means 1 mm, so the docking happens only 1 second later with respect to the case where the uncertainties were not considered.

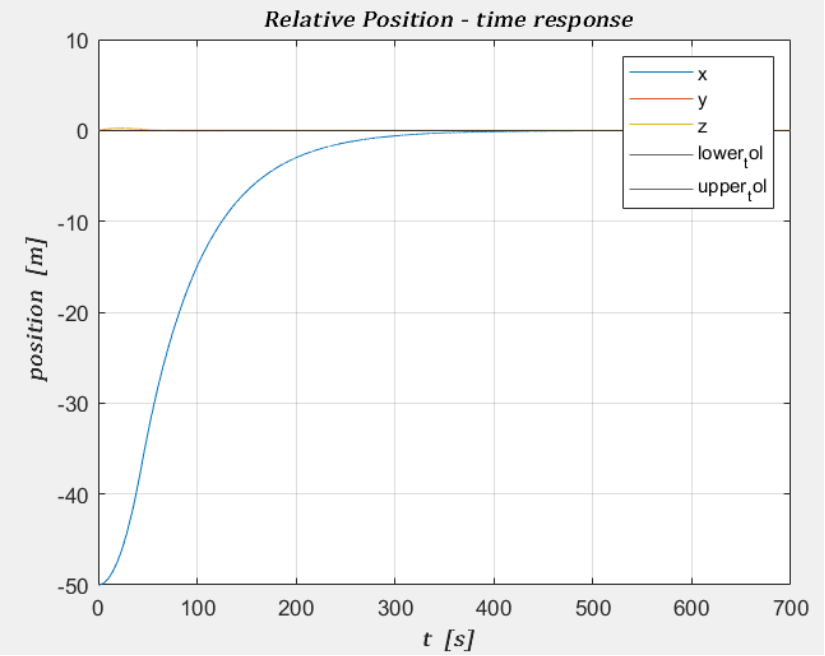

Figure 42 - Relative Position (parameter's perturbation)

In the next figure, after 442 s, the approach velocity reaches the value of 0.001 m/s, and it means that the approach velocity is of the order of the millimeter, so the tracking happens only 2 seconds after with respect the case without uncertainties.

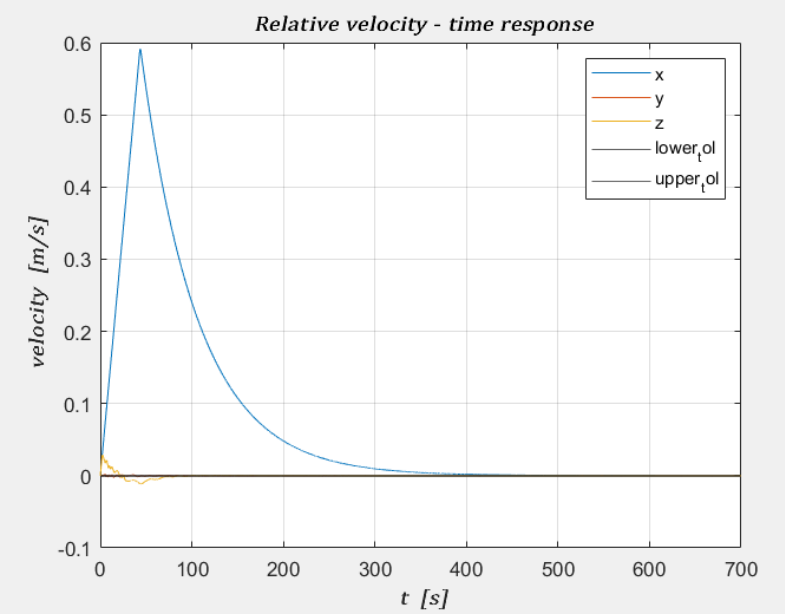

Figure 43 - Relative Velocity (parameter's perturbation)

The Tdc control input is similar to the previous case for apart the fact that the z coordinate reaches a higher value with respect the previous case.

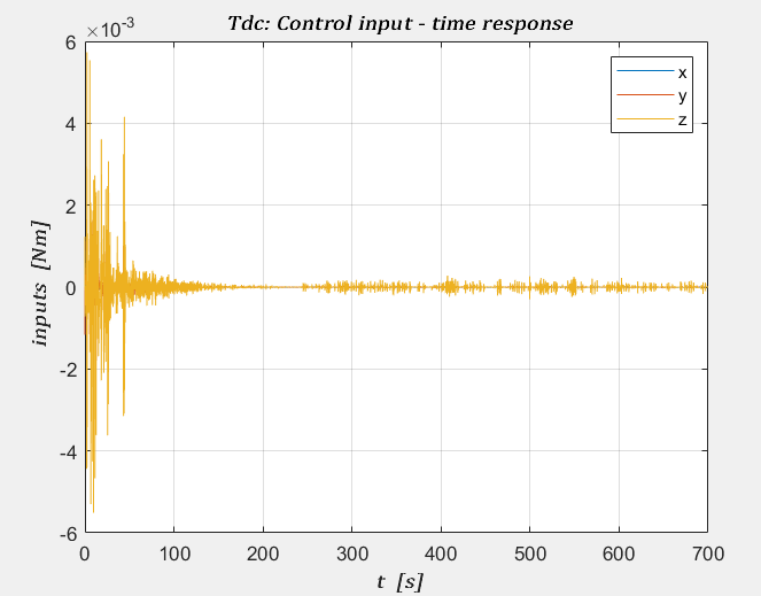

Figure 44 - Tdc: Control Input (parameter's perturbation)

The Fdc control input is similar to the previous case apart for the fact that the x coordinate reaches a higher value (-0.2) with respect the previous case without parameter's variations.

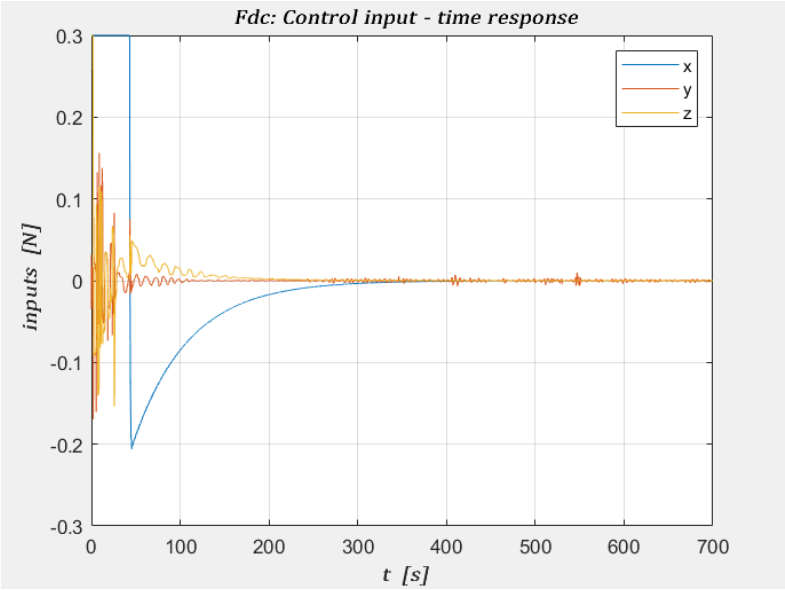

Figure 45 - Fdc: Control Input

5. Robust Analysis – Montecarlo simulations (V-bar approach)

In this section of the thesis has been analyzed the behavior of the system and its robustness considering different random initial conditions in a certain rage. The main objective is observing the obtained results and comparing them to the results obtained in the previous section (considering the non-linear plant and the linear model for the controller) where the initial conditions were fixed.

In this case it must be evaluated the reaction of the system to uncertainties in a large number of maneuvers with randomly different initial conditions.

In this section a total of 300 simulation has been performed, divided in 10 steps composed by 30 simulations each, considering larger errors on the uncertain parameters with a predefined magnitude on the initial condition of the uncertain parameters, that are mass, inertia, relative position, relative attitude, and angular velocity.

The first setup considered has been the following:

Step 1: 30 simulations with:

- random disturbance of amplitude $\mathbf{2.5 \cdot 10^{-1}}\ \boldsymbol{m}$ on relative position (all three axes);
- random disturbance of amplitude $\mathbf{2}\ \boldsymbol{kg}$ on the mass;
- random disturbance of amplitude $\mathbf{10}°$ on all three attitude angles;

- random disturbance of amplitude $\mathbf{0.2}\ \boldsymbol{rad/s}$ on angular velocity (all three axes).
- Random disturbance of the ***10%*** on the value of the inertia;

In those first 30 simulations is possible to see that the requirements on all the 4 state variables are respected.

The residual transient does not overcome 200 s of simulation and steady state values are ensured for each time response.

As is possible to observe in the next figure, the relative attitude has as max value almost 0.2 rad that means 11 deg, instead at the contact it is less than 1 deg, as it is required.

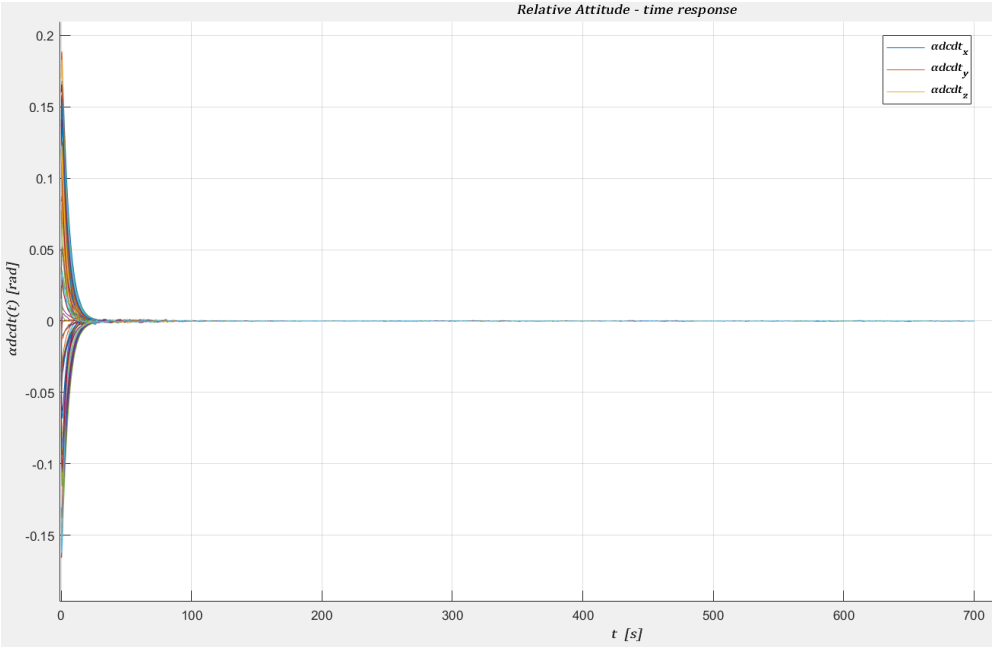

Figure 46 - Relative Attitude (Step 1 - Montecarlo simulation)

The relative angular velocity, at the contact is less than 0.1 deg/s, as it is required.

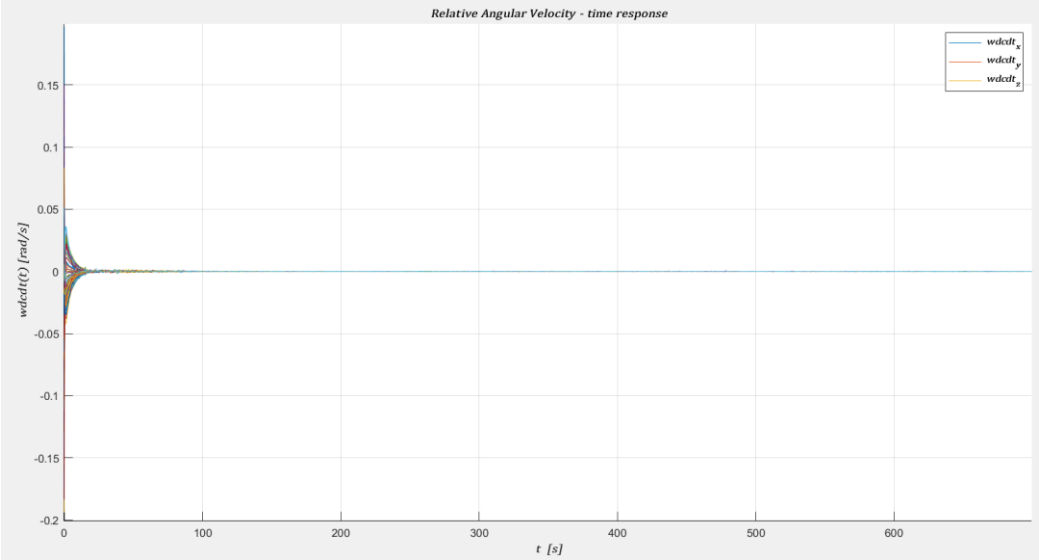

Figure 47 - Relative Angular Velocity (Step 1 - Montecarlo simulation)

After 550 s the relative position reaches the reference maintaining a value at the contact, on the docking axis of less than 0.01m as required.

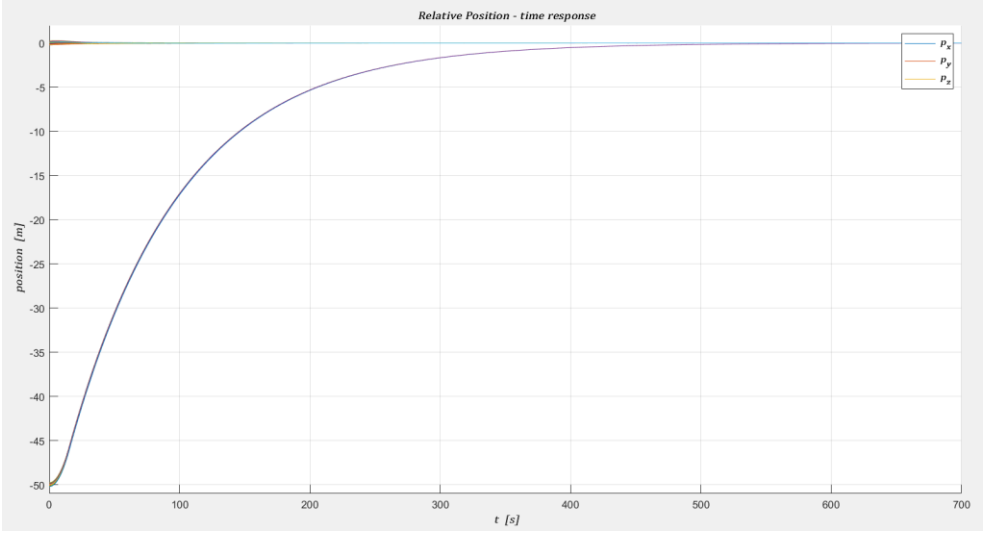

Figure 48 - Relative Position (Step 1 - Montecarlo simulation)

The relative velocity reaches a max value of 0.53 m/s, but at contact it does not overcome the imposed limit of 0.02 m/s on the approach velocity and of 0.01 m/s on the lateral velocity.

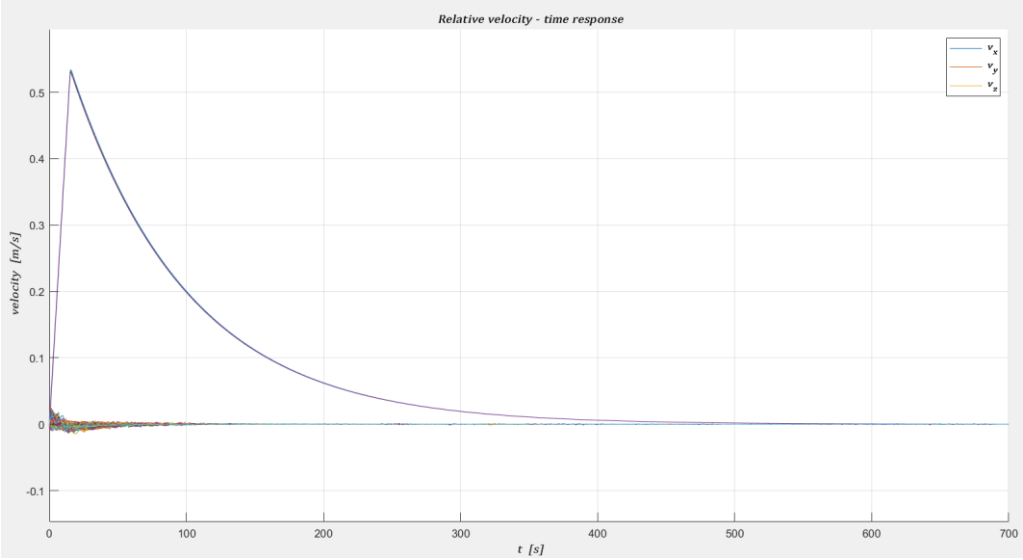

Figure 49 - Relative Velocity (Step 1 - Montecarlo simulation)

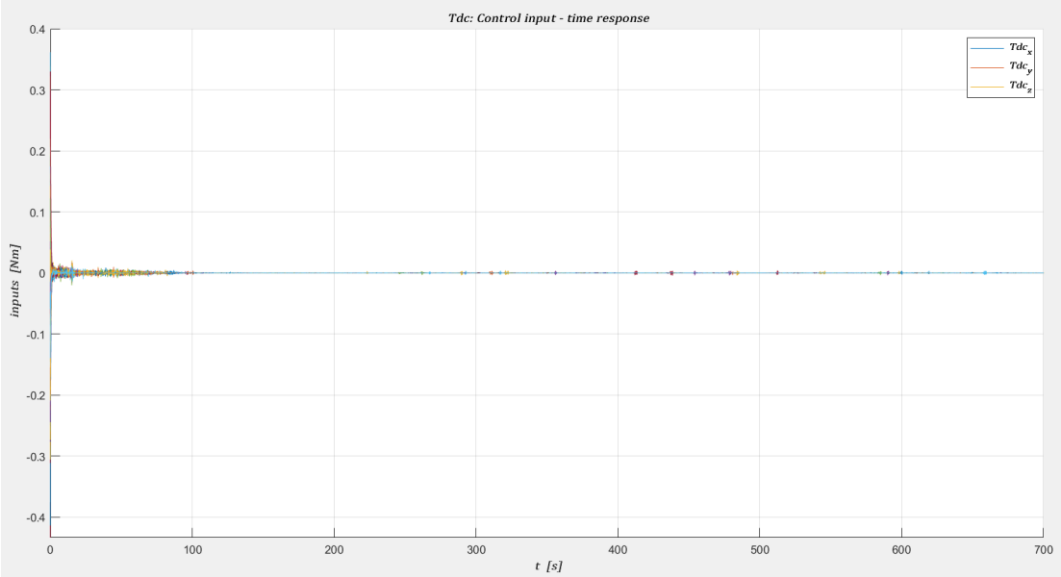

Figure 50 - Tdc: Control Input (Step 1 - Montecarlo simulation)

Is possible to observe that the Fdc control input is stuck to the saturation level for 25 seconds.

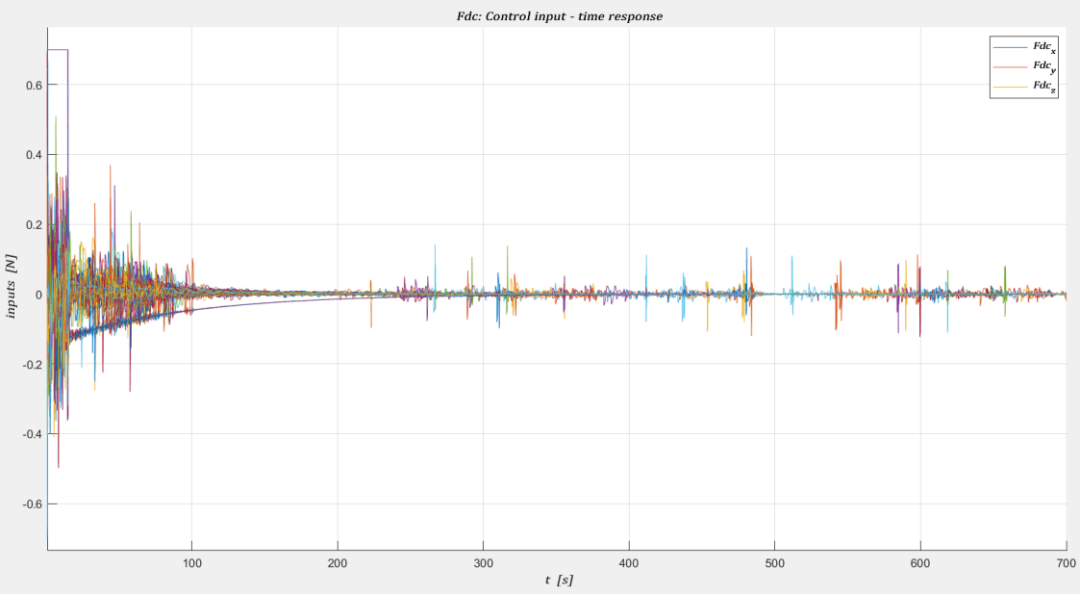

Figure 51 - Fdc: Control Input (Step 1 - Montecarlo simulation)

As seen in the previous simulations the obtained results are comparable to the ones obtained in the previous subchapter.

The control strategy is well optimized and able to ensure a robust behavior.

Step 2: 30 simulations with:

- random disturbance of amplitude $\mathbf{2.5}\ \boldsymbol{m}$ on relative position (all three axes);
- random disturbance of amplitude $\mathbf{2}\ \boldsymbol{kg}$ on the mass;
- random disturbance of amplitude $\mathbf{10}°$ on all three attitude angles;

- random disturbance of amplitude $\mathbf{0.2}\ \boldsymbol{rad/s}$ on angular velocity (all three axes).
- Random disturbance of the $\boldsymbol{10\%}$ on the value of the inertia;

As is evident in the next figure, no changes in the attitude behavior can be identified, as there is no further uncertainty added to the dynamics in this case with respect to the previous one.

The Relative attitude has as max value almost 0.2 rad that means 11 deg. After the first 150 s where the signal's behavior is a bit perturbed, it starts to settle to the reference of 0 degrees. At the contact the relative attitude is less than 1 deg, as it is required.

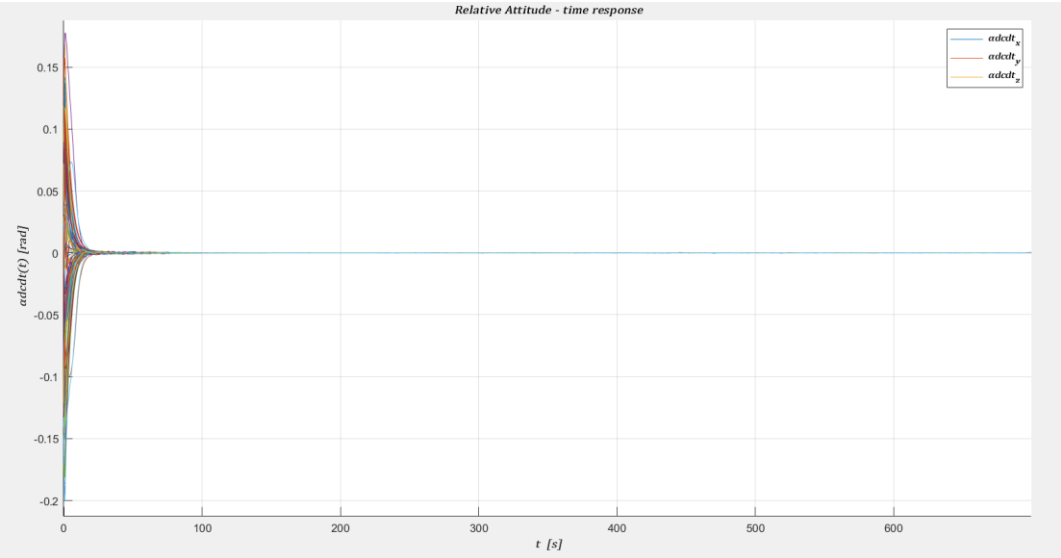

Figure 52 - Relative Attitude (Step 2 - Montecarlo simulation)

The Relative angular velocity has as max value almost 0.2 rad/s that means 11 deg/s. After the first 100 s where the signal's behavior is a bit perturbed, it starts

to settle to the reference of 0 degrees. At the contact the relative angular velocity is less than 0.1 deg/s, as it is required.

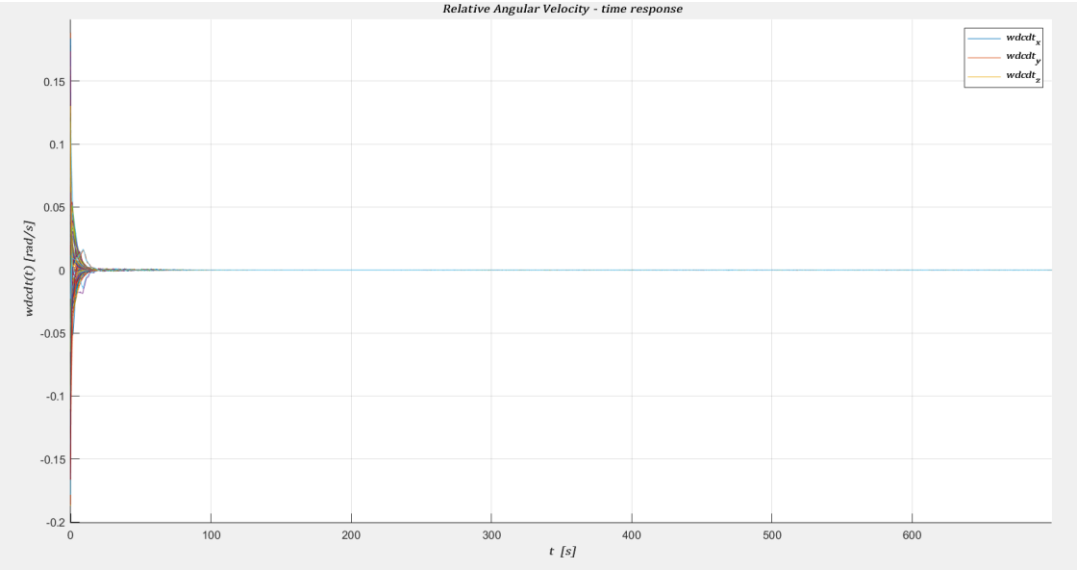

Figure 53 - Relative Angular Velocity (Step 2 - Montecarlo simulation)

In the relative position is possible to see that the initial position of the chaser varies in a certain range around 50 m of distance between the 2 spacecrafts. The result is optimal in fact, despite the big uncertainty considered in this case, the projected controller is able to control the system. The lateral alignment is of less than 0.01 m, as required.

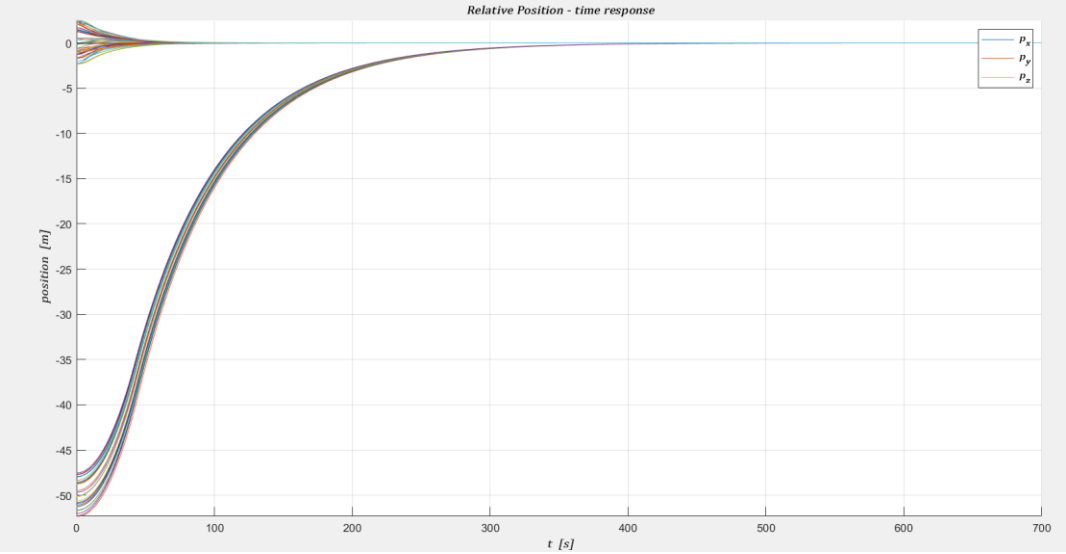

Figure 54 -- Relative Position (Step 2 - Montecarlo simulation)

The Relative velocity time response does not differ much with respect to the one observed in the previous step, it only becomes a bit more perturbed. The approach velocity at contact is less than 0.02 m/s at the end of docking and the lateral velocity (along V-bar) at contact is of less than 0.01 m/s.

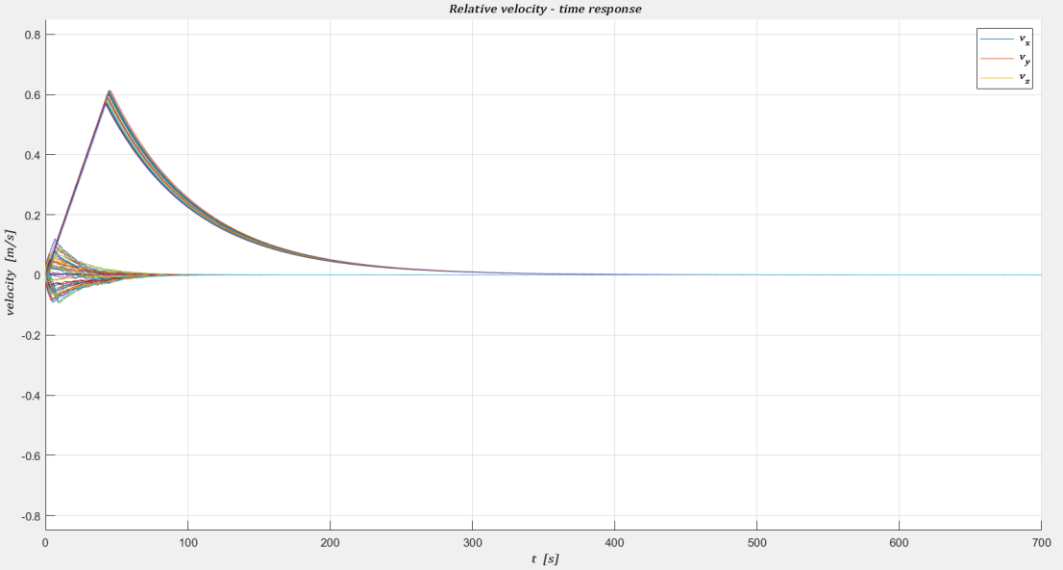

Figure 55 - Relative Velocity (Step 2 - Montecarlo simulation)

In the Tdc control input is observable an initial perturbed behavior of 80 s, then the behavior starts to settle to the reference.

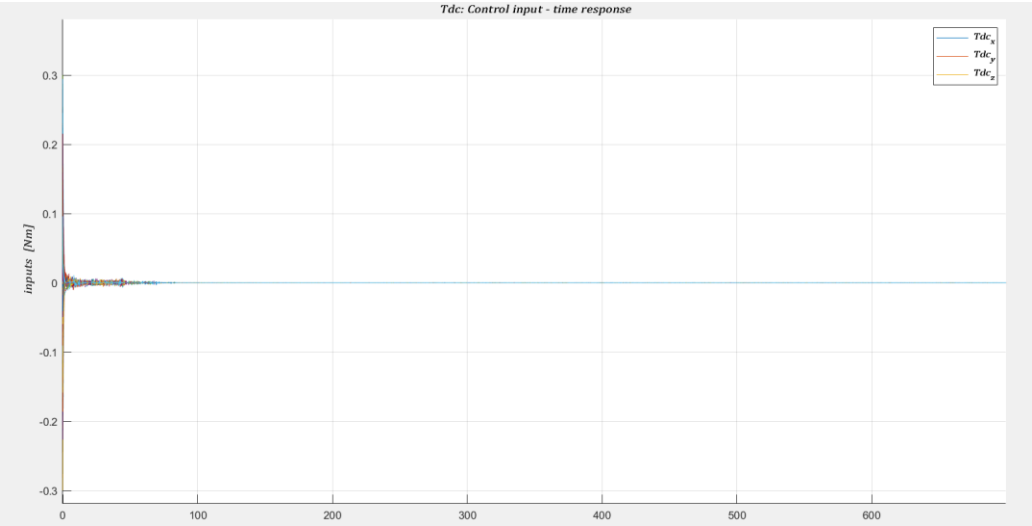

Figure 56 - Tdc: control input (Step 2 - Montecarlo simulation)

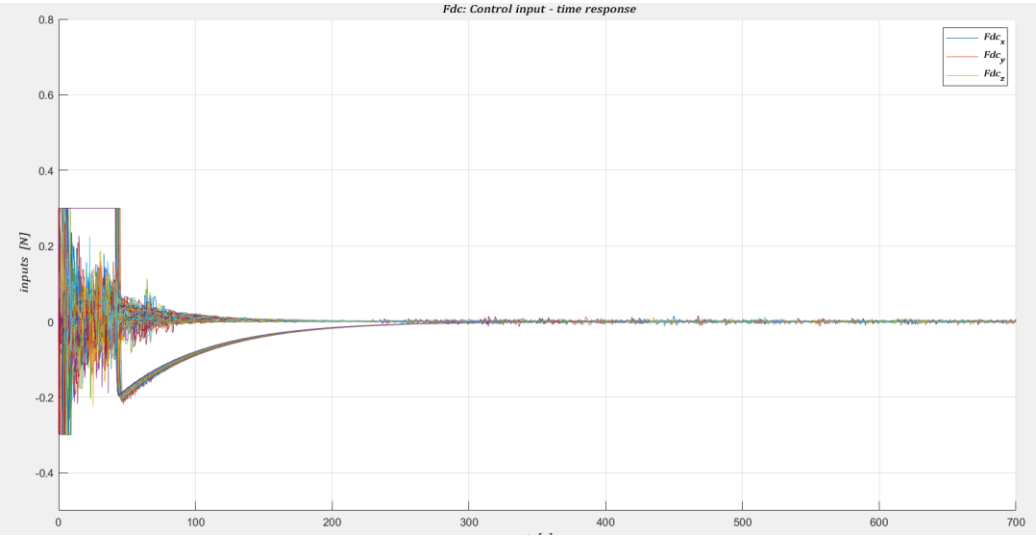

Figure 57 - Fdc: Control input (Step 2 - Montecarlo simulation)

Is possible to observe that the Fdc control input is stuck to the saturation level for 45 seconds showing a more severe condition to compensate in terms of uncertainties.

Conclusion

The use of small satellites is gaining great success in the New Space Economy thanks to their small size, low cost and reduced development time.

The definition of the system as has be done in this work, overcomes the limits of Hill's equations that are limited to define the relative motion between the chaser's barycenter the and target's barycenter and in addition, allows to design a single controller for both the rotational and the translational part.

In this thesis's work has been produced a control system, using a control strategy based on Model Predictive Control, able to meet the performance requirements for a CubeSat engaged in a Docking maneuver with another spacecraft.

Some of the future developments of greater interest for this work are: to introduce in simulative environment the actuators of the Cubesat (i.e. the propulsive system) which introduce further uncertainties and to consider the need to perform anti-collision maneuvers in case of failure or incorrect approach of the CubeSat towards Space Rider.

References

1. J. R. Kopacz, R. Herschitz, J. Roney, Small satellites an overview and assessment, Acta Astronautica, Volume 170, 2020, Pages 93-105, https://doi.org/10.1016/j.actaastro.2020.01.03 4.
2. Corpino S., Stesina F. (2020), Inspection of the cis-lunar station using multi-purpose autonomous Cubesats, Acta Astronautica, Volume 175, 2020, Pages 591-605, https://doi.org/10.1016/j.actaastro.2020.05.053 .
3. S Corpino, F Stesina, D Calvi, L Guerra, (2020), Trajectory analysis of a CubeSat mission for the inspection of an orbiting vehicle, Advances in aircraft and spacecraft science, Vol 7(3), pp 271-290, https://doi.org/10.12989/aas.2020.7.3.271
4. W. Fehse, Automated Rendezvous and Docking of Spacecraft, Pages 12-25

5. J. Bowen, M. Villa, A. Williams, CubeSat based Rendezvous, Proximity Operation, and Docking in the CPOD Mission
6. G. Naletto, A. Francesconi, M. Duzzi, Spacecraft Rendezvous and docking using electromagnetic interaction
7. Di Cairano, S. Park, H. Kolmanovsky (2012) "Model Predictive Control Approach for Guidance of Spacecraft Rendezvous and Proximity Maneuvering", *Int. Journal of Robust and Non Linear Control*, vol 22, DOI: 10.1002/rnc.2827
8. Camille Sébastien PIRAT (2018), Guidance, Navigation and Control for Autonomous Rendezvous and Docking of Nano-Satellites
9. Spacecraft Rendezvous and Docking Using Electromagnetic Interactions - Padua@Research (unipd.it)- Nella prima parte viene presentato

l’esperimento PACMAN (Position and Attitude Control with MAgnetic Navigation) il quale rappresenta un dimostratore tecnologico di un sistema di docking per piccoli satelliti basato su attuatori magnetici. Tale sistema, sviluppato all'interno del programma ESA Education Fly Your Thesis! 2017, è stato testato in gravità ridotta durante la 68th campagna di voli parabolici ESA a dicembre. La seconda parte si focalizza invece su un nuovo concept, TED (Tethered Electromagnetic Docking), secondo il quale le manovre di close-range rendezvous e docking possono essere realizzate lanciando una sonda elettromagnetica collegata ad un filo da un satellite chaser verso un’interfaccia elettromagnetica montata su di un satellite target. Stabilito il collegamento, tramite il recupero del filo, i due veicoli sono connessi rigidamente concludendo la manovra.

10. Avishai Weiss; Morgan BaldwinModel Predictive Control for Spacecraft Rendezvous and Docking: Strategies for Handling Constraints and Case Studies (5)
11. Model predictive control system design and implementation for spacecraft rendezvous, E.N. Hartley,P.A.Trodden, A.G. Richards, J.M. Maciejowski, Elsevier, 2012 (6)
12. Ebrahim Matter (Al-Gallaf) Member, IEEE, and A. Sultan Mohamed, Model Predictive Control Technique ANN Nonlinear Plants Modeling and Controller Synthesis (7)
13. Fabrizio Stesina, Tracking Model Predictive Control for docking maneuvers of a CubeSat with a big spacecraft (8)

Appendix 1

In this section, as seen in [8], with some modifications will be shared the Matlab code used to linearize the system.

Definition of variables for symbolic toolbox

syms alphaDCDT betaDCDT gammaDCDT dalphaDCDT dbetaDCDT dgammaDCDT real
P2P relative attitude angle variables

syms wxDCDT wyDCDT wzDCDT dwxDCDT dwyDCDT dwzDCDT real
P2P relative angular velocity variables

syms alphaDTo betaDTo gammaDTo dalphaDTo dbetaDTo dgammaDTo real
Target Docking port attitude variables

syms wxDTo wyDTo wzDTo dwxDTo dwyDTo dwzDTo real
Target relative angular velocity variables

syms ICDC11 ICDC12 ICDC13 ICDC21 ICDC22 ICDC23 ICDC31 ICDC32 ICDC33 mC real
Chaser Inertial parameters expressed in the docking port frame

```
syms ITDT11 ITDT12 ITDT13 ITDT21 ITDT22 ITDT23 ITDT31 ITDT32
ITDT33 real
```
Target Inertial parameters expressed in the docking port frame

```
syms rxDTDT ryDTDT rzDTDT rxDCDC ryDCDC rzDCDC real
```
Docking port positions expressed in the docking port frame

```
syms sxDT syDT szDT rT dsxDT dsyDT dszDT mu real
```
Relative position variables

```
syms TxDT TyDT TzDT TxDC TyDC TzDC FxDC FyDC FzDC real
```
Control Input

```
syms mu w0 real
```
Orbital parameters

```
syms aDT0 bDT0 cDT0 real
```
Linerization point

Kinematics P2P

```
AngleDC=[alphaDCDT ; betaDCDT ;gammaDCDT ] ;
cg=cos(gammaDCDT) ;
sg=sin(gammaDCDT) ;
cb=cos(betaDCDT ) ;
```

sb=sin(betaDCDT) ;

B_angle=1/cb *[cg -sg 0;

cb*sg cb*cg 0;

-sb*cg sb*sg cb] ;

dAngleDC=B_angle *[wxDCDT;wyDCDT;wzDCDT] ; *(5.a)*

Kinematics Target Orbital

AngleDTo=[alphaDTo ; betaDTo ; gammaDTo] ;

cg=cos(gammaDTo) ;

sg=sin(gammaDTo) ;

cb=cos(betaDTo) ;

sb=sin(betaDTo) ;

B_angle=1/cb *[cg -sg 0;

cb*sg cb*cg 0;

-sb*cg sb*sg cb] ;

dAngleDTo=B_angle *[wxDTo; wyDTo; wzDTo] ; *(5.b)*

Relative Dynamics

ICDC=[ICDC11 ICDC12 ICDC13 ;

ICDC21 ICDC22 ICDC23 ;

ICDC31 ICDC32 ICDC33] ;

ITDT=[ITDT11 ITDT12 ITDT13; ITDT21 ITDT22 ITDT23; ITDT31 ITDT32

ITDT33] ;

```
TDC=[TxDC TyDC TzDC]';
TDT=[TxDT TyDT TzDT]';

R1(alphaDTo)=[1 0 0; 0 cos(alphaDTo) -sin(alphaDTo); 0 sin(alphaDTo)
cos(alphaDTo)];
R2(betaDTo)=[cos(betaDTo) 0 sin(betaDTo); 0 1 0; -sin(betaDTo) 0
cos(betaDTo)];
R3(gammaDTo)=[cos(gammaDTo) -sin(gammaDTo) 0; sin(gammaDTo)
cos(gammaDTo) 0; 0 0 1];
ADTo=R3(gammaDTo)*R2(betaDTo)*R1(alphaDTo) ;

R1(alphaDCDT)=[1 0 0; 0 cos(alphaDCDT) -sin(alphaDCDT); 0
sin(alphaDCDT) cos(alphaDCDT)];
R2(betaDCDT)=[cos(betaDCDT) 0 sin(betaDCDT); 0 1 0; -sin(betaDCDT) 0
cos(betaDCDT)];
R3(gammaDCDT)=[cos(gammaDCDT) -sin(gammaDCDT) 0;
sin(gammaDCDT) cos(gammaDCDT) 0; 0 0 1];
ADCDT=R3(gammaDCDT)*R2(betaDCDT)*R1(alphaDCDT);

wDTo=[wxDTo; wyDTo; wzDTo] ;
wDCDT=[wxDCDT;wyDCDT;wzDCDT] ;
wo=[0 -w0 0]';
wIT=wDTo+ADTo*wo
```

Dynamics for attitude DTO

```
dwDTo=ITDT\(TDT-skew(wIT)*(ITDT*wIT))  (3.b)
dwxDTo=dwDTo(1) ;
dwyDTo=dwDTo(2) ;
dwzDTo=dwDTo(3) ;
```

Dynamics for attitude DCDT

```
dwDC=ICDC\(TDC-skew(wDCDT+ADCDT*wIT )
*(ICDC*(wDCDT+ADCDT*wIT ) ) )-(skew(-
wDCDT)*(ADCDT*wDTo)+ADCDT*dwDTo) ;  (2)
dwxDCDT=dwDC( 1 ) ;
dwyDCDT=dwDC( 2 ) ;
dwzDCDT=dwDC( 3 ) ;
```

P2P Translation dynamics

```
rTo =[ 0; 0; - rT ] ;
sDCDT=[sxDT ; syDT ; szDT ] ;
dsDCDT=[dsxDT ; dsyDT ; dszDT ] ;
rDCDC=[rxDCDC; ryDCDC; rzDCDC ] ;
rDTDT=[rxDTDT; ryDTDT; rzDTDT ] ;
rDCDT=ADCDT'*rDCDC;
rxCDT=rDCDT( 1 ) ;
ryCDT=rDCDT( 2 ) ;
```

```
rzCDT=rDCDT( 3 ) ;
FDC=[FxDC FyDC FzDC]';
rcDT=ADTo*rTo+sDCDT-rDCDT+rDTDT;
accDT=mu*ADTo*rTo/norm (ADTo*rTo ) ^3 -mu*(rcDT ) /norm ( rcDT
)^3+ADCDT'*FDC/mC;
s=sDCDT-rDCDT+rDTDT;
ddsDCDT=-skew (dwDTo)*s ...
- skew (wDTo)*skew (wDTo)*s ...
-skew (ADTo*wo )*skew (ADTo*wo )*s ...
-2*skew (wDTo)*dsDCDT ...
-2*skew (ADTo*wo )*dsDCDT ...
-2*skew (ADTo*wo )*skew (wDTo)*s ...
+2*skew (ADTo*wo+wDTo)*skew (ADCDT'*wDCDT) *(rDCDT) ...
+accDT ...
+skew (ADCDT'*dwDC) *(rDCDT) ...
+2*skew (ADCDT'*wDCDT)*skew (ADCDT'*wDCDT)*rDCDT;
```

Computation of the Jacobian matrix

```
ftot =[dAngleDC ;dwDC; dsDCDT; ddsDCDT ] ;
A =jacobian( ftot , [ AngleDC' wDCDT' sDCDT' dsDCDT'])
B =jacobian( ftot , [ TDC' FDC'])
```

Linearization

```
alphaDCDT=0;
betaDCDT=0;
gammaDCDT=0;
wxDCDT=0;
wyDCDT=0;
wzDCDT=0;
alphaDTo=0;
betaDTo=0;
gammaDTo=0;
wxDTo=0;
wyDTo=0;
wzDTo=0;
TxDC=0;
TyDC=0;
TzDC=0;
TxDT=0;
TyDT=0;
TzDT=0;
sxDT=0;
syDT=0;
szDT=0;
dsxDT=0;
dsyDT=0;
dszDT=0;
FxDC=0;
FyDC=0;
FzDC=0;
```

Chaser mass properties

mC=20; *[Kg] - Chaser mass*

mC=mC+(4*rand-2); *Disturbed chaser mass*

m=mC;

Cb=0.0011; *Basilistic coefficient*

base=0.226; *[m]*

height =0.20; *[m]*

depth=0.366; *[m]*

Face_1=base*height; *[m^2]*

Face_2=base* depth; *[m^2]*

Face_3= height*depth;

Cd=2; *drag coefficient*

Ix=(base*base+ height*height)*m/12; *[kg*m^2]-moment of Inertia with respect to X axis*

Iy=(height*height+depth*depth)*m/12; *[kg*m^2]-moment of Inertia with respect to Y axis*

Iz=(base*base+ depth * depth)*m /12; *[kg*m^2]-moment of Inertia with respect to Z axis*

Isc=[Ix 0 0;0 Iy 0; 0 0 Iz];

Idc=Isc+m*[0 0 0; 0 (base/2)^2 0; 0 0 (base/2)^2];

ICDC11=Idc(1,1);

ICDC12=Idc(1,2);

ICDC13=Idc(1,3);

ICDC21=Idc(2,1);

ICDC22=Idc(2,2);

ICDC23=Idc(2,3);

ICDC31=Idc(3,1);

ICDC32=Idc(3,2);

ICDC33=Idc(3,3);

Target mass properties

mT = 2000; *[Kg]*

T_Ix=1500; *[Kg/m^2]*

T_Iy=1100; *[Kg/m^2]*

T_Iz=1100; *[Kg/m^2]*

T_Inertia = [T_Ix 0 0; 0 T_Iy 0; 0 0 T_Iz];

Idt=T_Inertia+mT*[0 0 0; 0 (base/2)^2 0; 0 0 (base/2)^2]

ITDT11=Idt(1,1);

ITDT12=Idt(1,2);

ITDT13=Idt(1,3);

ITDT21=Idt(2,1);

ITDT22=Idt(2,2);

ITDT23=Idt(2,3);

ITDT31=Idt(3,1);

ITDT32=Idt(3,2);

```
ITDT33=Idt(3,3);

mu = 3.986 *10^14;    [m^3/s^2] - earth gravitational constant
Rearth=6.378137e6;   [m] - Earth radius
h=828e3;                  [m] - altitude of the orbit
rT=Rearth+h             [m] - target position(constant for reference circular
orbits)
rTo =[ 0; 0; - rT ];
w0=sqrt(mu/norm(rTo)^3)
```

Initial conditions

```
AngleDC=[0 0 0]'; alphaDCD=AngleDC(1) ; betaDCDT
=AngleDC(2);gammaDCDT=AngleDC(3);
AngleDTo=[0 0 0]';alphaDTo=AngleDTo(1) ; betaDTo=AngleDTo(2) ;
gammaDTo=AngleDTo(3);
rDCDC=[0.15 0 0]';rxDCDC=rDCDC(1); ryDCDC=rDCDC(2);
rzDCDC=rDCDC(3);
rDTDT=[-0.15 0 0]';rxDTDT=rDTDT(1); ryDTDT=rDTDT(2);
rzDTDT=rDTDT(3);
sDCDT=[-50 0 0]';sxDT=sDCDT(1); syDT=sDCDT(2) ; szDT=sDCDT(3);
wDTo=[0 0 0]';wxDTo=wDTo(1); wyDTo=wDTo(2); wzDTo =wDTo(3);
wDCDT=[0 0 0]';wxDCDT=wDCDT(1); wyDCDT=wDCDT(2);
wzDCDT=wDCDT(3);

A = eval(A);
B = eval(B);
```

```
A = simplify(A);
B = simplify(B);
```

Appendix 2

In this section, the Matlab function used to represent the non-linear system is reported:

```
function f = non_linear_system(x,u)
f = zeros(12,1);
```

Dynamics for attitude

```
w0 = 0.0010;
 alphaDTo = 0;
 betaDTo = 0;
 gammaDTo = 0;
R1=[1 0 0; 0 cos(alphaDTo) -sin(alphaDTo); 0 sin(alphaDTo) cos(alphaDTo)];
R2=[cos(betaDTo) 0 sin(betaDTo); 0 1 0; -sin(betaDTo) 0 cos(betaDTo)];
R3=[cos(gammaDTo) -sin(gammaDTo) 0; sin(gammaDTo) cos(gammaDTo) 0;
0 0 1];
ADTo=R3*R2*R1;

wDTo = zeros(3,1);
```

```
wo=[0 -w0 0]';
wIT=wDTo+ADTo*wo
ITDT=1.0e+03*[1.5000 0 0; 0 1.1255 0;0 0 1.1255];

TxDT=0; TyDT=0; TzDT=0;
TDT=[TxDT TyDT TzDT]';
wxDTo=0; wyDTo=0; wzDTo=0;
wDTo=[wxDTo wyDTo wzDTo]';
dwDTo = ITDT\(TDT-skew(wIT)*(ITDT*wIT))
dwxDTo=dwDTo(1) ;
dwyDTo=dwDTo(2) ;
dwzDTo=dwDTo(3) ;

f(4,:) = dwDTo;
```

P2P Translation dynamics

```
rDCDC = [0.15; 0; 0];
rDTDT = [-0.15 0 0]';
AngleDC= x(1:3,:);
alphaDCDT = x(1,:);
betaDCDT = x(2,:);
gammaDCDT = x(3,:);

R1dcdt = [1 0 0; 0 cos(alphaDCDT) -sin(alphaDCDT); 0 sin(alphaDCDT)
cos(alphaDCDT)];
```

```
R2dcdt=[cos(betaDCDT) 0 sin(betaDCDT); 0 1 0; -sin(betaDCDT) 0
cos(betaDCDT)];
R3dcdt=[cos(gammaDCDT) -sin(gammaDCDT) 0; sin(gammaDCDT)
cos(gammaDCDT) 0; 0 0 1];
ADCDT=R3dcdt*R2dcdt*R1dcdt ;

rDCDT=ADCDT'*rDCDC;
sDCDT=x(7:9,:);
s=sDCDT-rDCDT+rDTDT;

dsDCDT=x(10:12,:);
dsxDT=x(10,:);
dsyDT=x(11,:);
dszDT=x(12,:);
f(7:9,:)=x(10:12,:)
wDCDT=x(4:6,:);

mu = 3.986 *10^14;
Rearth=6.378137e6; h=828e3; rT=Rearth+h;
mC=20;
rTo =[ 0; 0; - rT ] ;
sDCDT=x(7:9,:);
sxDT=x(7,:);
syDT=x(8,:);
szDT=x(9,:);
sDCDT=[sxDT ; syDT ; szDT ] ;
dsDCDT=[dsxDT ; dsyDT ; dszDT ] ;
```

```
rDCDT=ADCDT'*rDCDC;
rxCDT=rDCDT( 1 ) ;
ryCDT=rDCDT( 2 ) ;
rzCDT=rDCDT( 3 ) ;
FDC=u(4:6,:);
FxDC=u(4,:);
FyDC=u(5,:);
FzDC=u(6,:);
FDC=[FxDC FyDC FzDC]';
rcDT=ADTo*rTo+sDCDT-rDCDT+rDTDT;
accDT=mu*ADTo*rTo/norm (ADTo*rTo ) ^3 -mu*(rcDT ) /norm ( rcDT
)^3+ADCDT'*FDC/mC;
```

Absolute docking ports dynamics

```
ICDC =[0.1641 0  0; 0  0.5896  0; 0  0 0.6095];
TDC=u(1:3,:);
TxDC=u(1,:);
TyDC=u(2,:);
TzDC=u(3,:);

dwDC=ICDC\(TDC-skew(wDCDT+ADCDT*wIT )
*(ICDC*(wDCDT+ADCDT*wIT ) ) ) ...
-(skew(-wDCDT)*(ADCDT*wDTo)+ADCDT*dwDTo) ;
dwxDCDT=dwDC( 1 ) ;
dwyDCDT=dwDC( 2 ) ;
dwzDCDT=dwDC( 3 ) ;
```

```
f(4:6,:)=dwDC;

ddsDCDT=-skew (dwDTo)*s ...
- skew (wDTo)*skew (wDTo)*s ...
-skew (ADTo*wo )*skew (ADTo*wo )*s ...
-2*skew (wDTo)*dsDCDT ...
-2*skew (ADTo*wo )*dsDCDT ...
-2*skew (ADTo*wo )*skew (wDTo)*s ...
+2*skew (ADTo*wo+wDTo)*skew (ADCDT'*wDCDT) *(rDCDT) ...
+accDT ...
+skew (ADCDT'*dwDC) *(rDCDT) ...
+2*skew (ADCDT'*wDCDT)*skew (ADCDT'*wDCDT)*rDCDT;

f(10:12,:)=ddsDCDT;
```

P2P Kinematics

```
AngleDC=[alphaDCDT ; betaDCDT ;gammaDCDT ] ;
cg=cos(gammaDCDT) ;
sg=sin(gammaDCDT) ;
cb=cos(betaDCDT ) ;
sb=sin(betaDCDT ) ;
B_angle=1/cb *[ cg -sg 0;
cb*sg cb*cg 0;
-sb*cg sb*sg cb ] ;
wxDCDT=x(4,:);
wyDCDT=x(5,:);
```

```
wzDCDT=x(6,:);
dAngleDC=B_angle *[wxDCDT;wyDCDT;wzDCDT] ;

f(1:3,:)=dAngleDC;
```

Kinematics Target Orbital

```
AngleDTo=[alphaDTo ; betaDTo ; gammaDTo ] ;
cg=cos(gammaDTo) ;
sg=sin(gammaDTo) ;
cb=cos( betaDTo ) ;
sb=sin( betaDTo ) ;
B_angle=1/cb *[cg -sg 0;
cb*sg cb*cg 0;
-sb*cg sb*sg cb ] ;
dAngleDTo=B_angle *[wxDTo; wyDTo; wzDTo] ;
```